AD

TECHNICAL REPORT ARCCB-TR-02016

CHARACTERIZATION OF EXPLOSIVELY BONDED AND FIRED TANTALUM LINERS APPLIED TO 25-MM GUN TUBES

C. MULLIGAN
M. AUDINO
P. COTE
G. KENDALL
C. RICKARD
S. SMITH
M. TODARO

NOVEMBER 2002

US ARMY ARMAMENT RESEARCH,
DEVELOPMENT AND ENGINEERING CENTER
Close Combat Armaments Center
Benét Laboratories
Watervliet, NY 12189-4000

DISCLAIMER

The findings in this report are not to be construed as an official Department of the Army position unless so designated by other authorized documents.

The use of trade name(s) and/or manufacturer(s) does not constitute an official endorsement or approval.

DESTRUCTION NOTICE

For classified documents, follow the procedures in DoD 5200.22-M, Industrial Security Manual, Section II-19, or DoD 5200.1-R, Information Security Program Regulation, Chapter IX.

For unclassified, limited documents, destroy by any method that will prevent disclosure of contents or reconstruction of the document.

For unclassified, unlimited documents, destroy when the report is no longer needed. Do not return it to the originator.

REPORT DOCUMENTATION PAGE

Form Approved
OMB No. 0704-0188

1. AGENCY USE ONLY (*Leave Blank*)	2. REPORT DATE	3. REPORT TYPE AND DATES COVERED
	November 2002	Final

4. TITLE AND SUBTITLE
CHARACTERIZATION OF EXPLOSIVELY BONDED AND FIRED TANTALUM LINERS APPLIED TO 25-MM GUN TUBES

5. FUNDING NUMBERS
AMCMS No. 6226.24.H191.1

6. AUTHORS
C. Mulligan, M. Audino, P. Cote, G. Kendall,
C. Rickard, S. Smith, and M. Todaro

7. PERFORMING ORGANIZATION NAME(S) AND ADDRESS(ES)
U.S. Army ARDEC
Benet Laboratories, AMSTA-AR-CCB-O
Watervliet, NY 12189-4000

8. PERFORMING ORGANIZATION REPORT NUMBER
ARCCB-TR-02016

9. SPONSORING / MONITORING AGENCY NAME(S) AND ADDRESS(ES)
U.S. Army ARDEC
Close Combat Armaments Center
Picatinny Arsenal, NJ 07806-5000

10. SPONSORING / MONITORING AGENCY REPORT NUMBER

11. SUPPLEMENTARY NOTES

12a. DISTRIBUTION / AVAILABILITY STATEMENT
Approved for public release; distribution unlimited.

12b. DISTRIBUTION CODE

13. ABSTRACT *(Maximum 200 words)*

Characterization analyses were conducted on sections taken from three truncated 25-mm gun tubes that were explosively bonded with pure tantalum. Two of the barrels had been test fired and one was received in the pre-fired condition. The two test-fired tubes consist of one smoothbore design and one no-twist rifled bore design. The specimen received in the pre-fired condition was the smoothbore design. Characterization work included macroscopic examination, liner thickness measurements, microstructural analysis, microhardness testing, adhesion testing, scanning electron microscopy, energy dispersive spectroscopy, wavelength dispersive spectroscopy, hydrogen analysis, and pulsed laser heating. Characterization results indicate vast improvement over the erosion characteristics of standard nitrided 25-mm Bushmaster gun tubes when firing the unfielded, original M919 propellant (100% HE 9053). Some areas of concern in the performance of the liner include heavy heat-check cracking, severe gas erosion, high concentration levels of hydrogen, and surface oxidation of the tantalum liners.

14. SUBJECT TERMS
Explosive Bonding, Tantalum. 25-mm Gun Tubes,
Wear, Erosion, Refractory Coatings

15. NUMBER OF PAGES
40

16. PRICE CODE

17. SECURITY CLASSIFICATION OF REPORT	18. SECURITY CLASSIFICATION OF THIS PAGE	19. SECURITY CLASSIFICATION OF ABSTRACT	20. LIMITATION OF ABSTRACT
UNCLASSIFIED	UNCLASSIFIED	UNCLASSIFIED	UL

TABLE OF CONTENTS

TABLES

LIST OF ILLUSTRATIONS

ACKNOWLEDGEMENTS

The authors would like to thank L. Bohojckeek and T. Sage for metallographic preparation and S. Lee for x-ray fluorescence data.

BACKGROUND

Three truncated 25-mm Bushmaster gun tubes were fabricated and explosively bonded with tantalum by Technology to Products on the Leading Edge, Inc. (TPL) as part of an Army Research Office (ARO) Small Business Innovative Research (SBIR) Phase II effort. The tubes had to be shortened in order to facilitate the explosive bonding process. The highly tapered design of the standard Bushmaster gun tubes may lead to deformation or rupture of the muzzle end during the explosive bonding process. Following fabrication, the tubes were sent to the U.S. Army Aberdeen Test Center (ATC) at Aberdeen Proving Ground, MD, for test firing. Tube B (smoothbore design) was test fired using a total of 1385 rounds M919 APFSDS-T ammunition. This ammunition was never fielded due to its high flame temperature and condemnation of nitrided Bushmasters in fewer than 300 rounds. Tube C (no-twist rifled design) was test fired using a total of 600 rounds of this same ammunition. Tube A (smoothbore design) was not test fired. Benét Laboratories received several sections from all three tubes (Figure 1). The sections received from Tube A consisted of three full rings approximately 1-inch in length. The sections from Tubes B and C, consisted of three half rings each (~2 inches in length), and one quarter ring each (~4 inches in length). The 4-inch length quarter rings were taken in the areas of the most severe erosion in each tube, namely, 6 to 10 inches and 4.5 to 8.5 inches, in Tubes B and C, respectively.

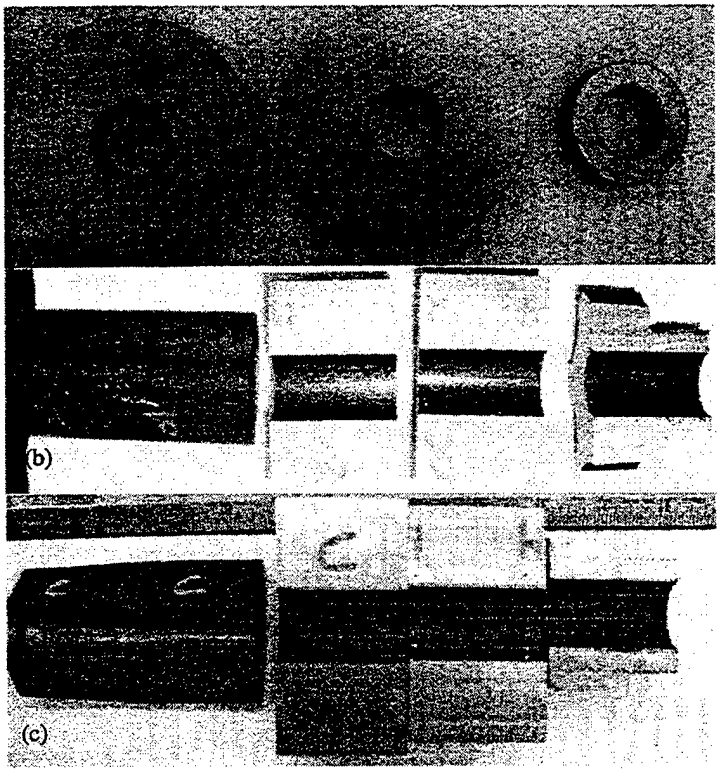

Figure 1. As-received sections of (a) Tube A, (b) Tube B, and (c) Tube C.

CHARACTERIZATION PROCEDURE

All specimens provided were subjected to a characterization protocol based upon Benét Laboratories established protocol for protective coatings. The specific characterizations performed on these specimens were:

- Macroscopic examination
- Liner thickness measurement
- Microstructural analysis including microhardness
- Adhesion testing
- Scanning electron microscopy (SEM) and energy dispersive spectroscopy (EDS)
- Hydrogen analysis
- Wavelength dispersive spectroscopy (WDS)
- Pulsed laser heating

The results of these tests are described below.

MACROSCOPIC EXAMINATION

Tube A (Smoothbore-Unfired)

The surface of Tube A was smooth and reflective with the exception of tooling marks that ran parallel to the axis of the tube. The crosshatched pattern left from the honing operation was readily visible to the naked eye. No large-scale defects were discernable in the main bore. Toward the muzzle end there were some irregularities in the surface of the liner. It appears that areas of the liner in this region were not thick enough to completely fill in the liner subsequent to honing. This did not seem to be detrimental to the performance of the liner as the same features, unaffected, are seen in Tube B post-firing (Figure 2).

Figure 2. Surface coating at muzzle end of smoothbore Tube B; note defects on surface.

Tube B (Smoothbore-Fired)

The most predominant erosion patterns of Tube B were readily distinguishable with visual and stereomicroscopic examination. Heavy heat-checking and thermomechanical/ thermochemical damage of the coating is evident at the 6- to 10-inch location, along with the development of deep erosion troughs that extend well into the steel (Figures 3 and 4).

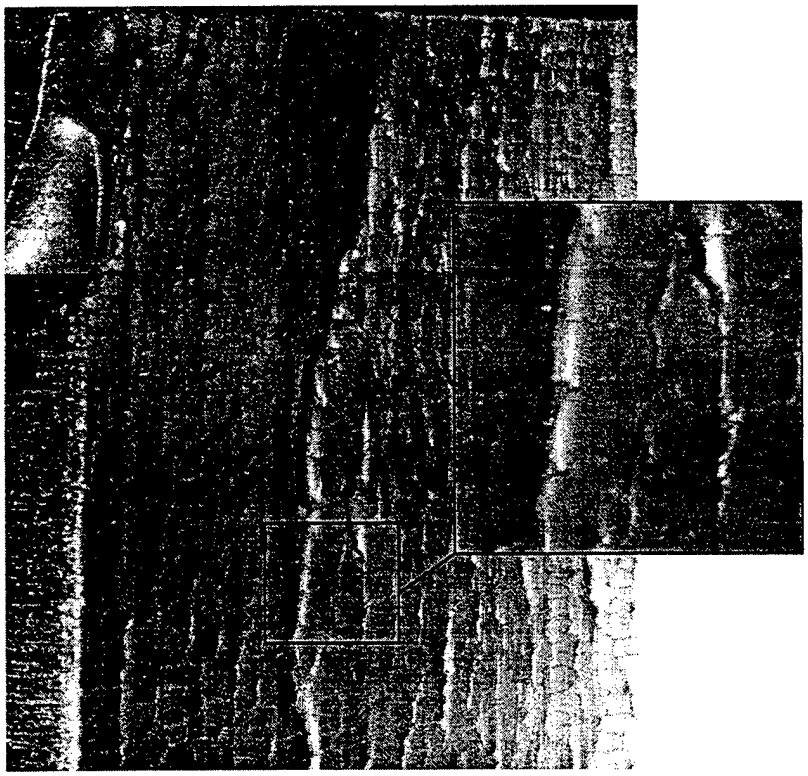

Figure 3. Severe heat-checking and gas erosion exhibited at the 6.5-inch location of Tube B.

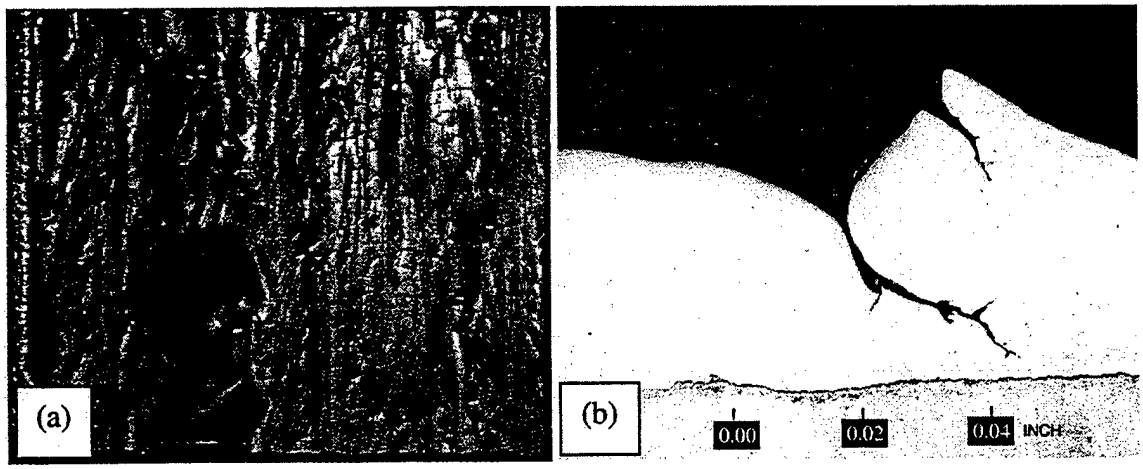

Figure 4. (a) Severe heat-checking and gas erosion exhibited at 8 inches from the rear face of the tube (RFT), and (b) cross-section of Tube B at 50X.

Heat-checking was also evident at the 12- to 14-inch location, along with a general surface roughening as shown in Figure 5a. This roughening is due to the cracking followed by some plastic flow and erosion in this area. This was confirmed by metallographic observations made at this location (Figure 5b).

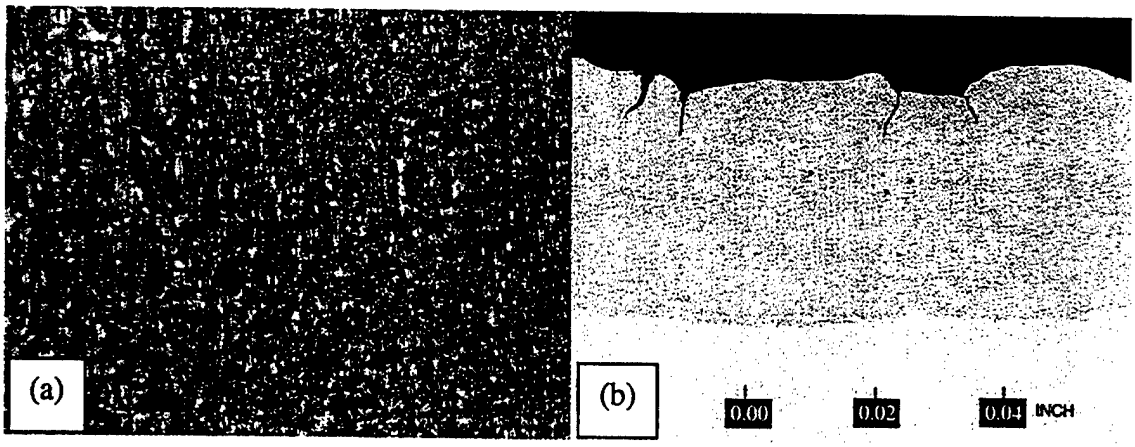

Figure 5. (a) Surface roughening exhibited at 12 to 14 inches from RFT, and (b) cross-section of Tube B at 50X.

Acute surface roughening was seen in the 18- to 20-inch location (Figure 6). Upon metallographic examination, it was found that cracking also contributed to roughness at this location. Here, the cracks are more finely spaced and shallower than in the locations closer to the breech.

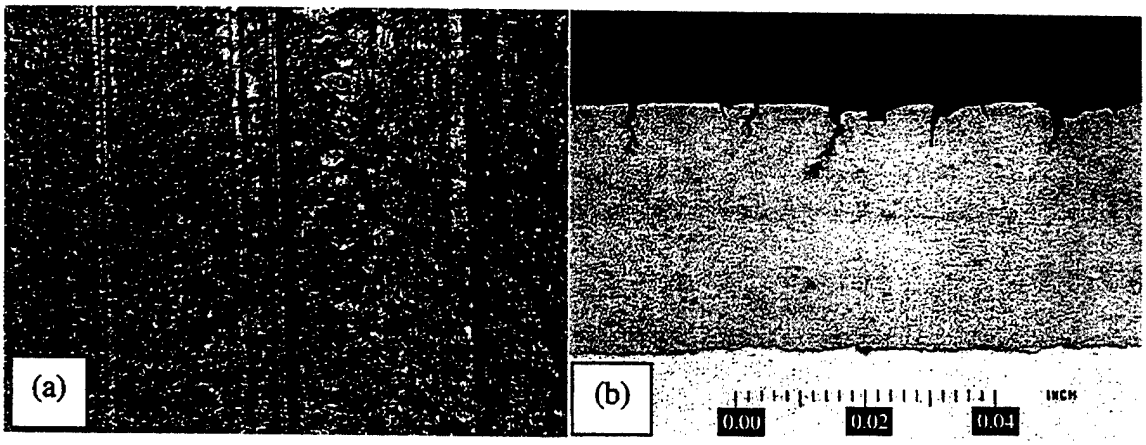

Figure 6. (a) General surface roughening seen at 18 to 20 inches from RFT, and (b) longitudinal cross-section of Tube B at 50X.

The liner at the muzzle end (38- to 40-inch location) was virtually unperturbed by the firing.

Tube C (No-Twist/Rifled-Fired)

The most dominant feature of the Tube C specimens was severe erosion of the lands up to about 16 inches from RFT (Figures 7 and 8), including near complete obliteration nearest the origin-of-rifling (4- to 8-inch location). Also, seen in the liner of the 4- to 8-inch section were heavy heat-checking and stress patterns similar to those observed in Tube B.

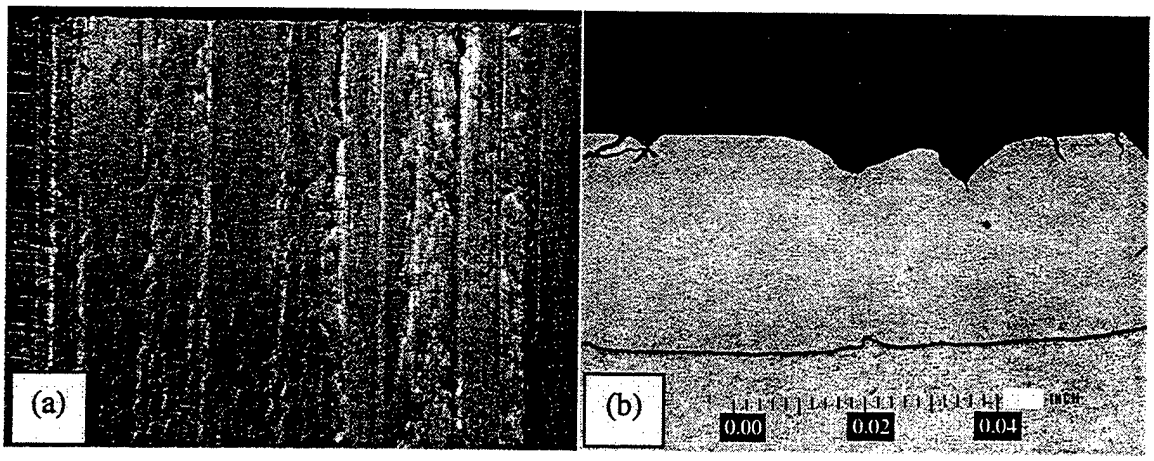

Figure 7. (a) Heat-checking and land erosion at 4 to 8 inches from RFT, and (b) cross-section of Tube C at 50X.

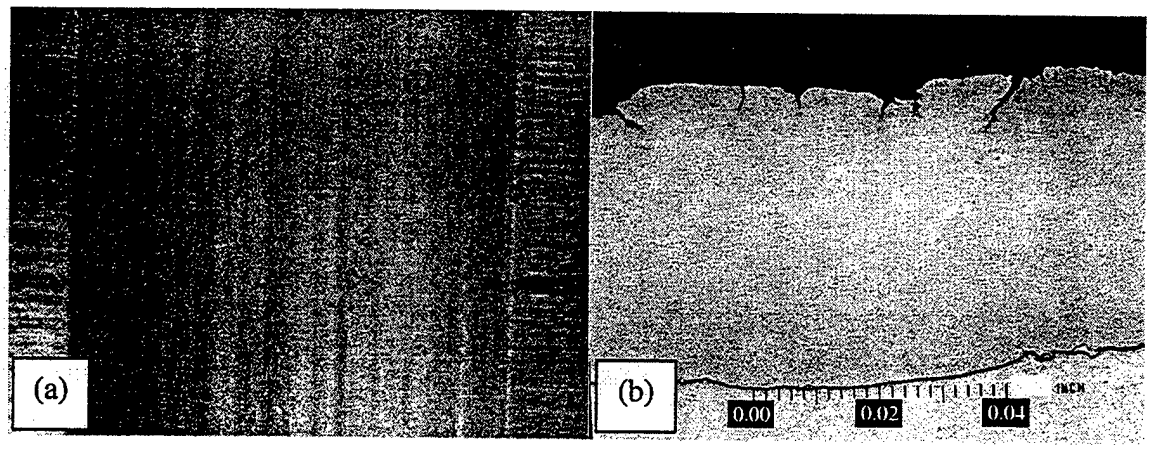

Figure 8. (a) Surface roughening and land erosion at 14 to 16 inches from RFT, and (b) cross-section of Tube C at 50X.

Besides the heavy wear and erosion seen in the main bore in the 14- to 16-inch location, there occurred a general roughening similar to that of Tube B. As with Tube B, this roughening seemed to occur due to cracking of the coating at the surface, followed by deformation and preferential erosion within the cracks (Figure 8b).

A general roughening of the surface in the 28- to 30-inch location was also observed (Figure 9a). The roughening observed here is due to both cracking and loss of the coating at what appears to be an interfacial phase formed from the dual explosive bonding process (Figure 9b), which will be discussed in a later section.

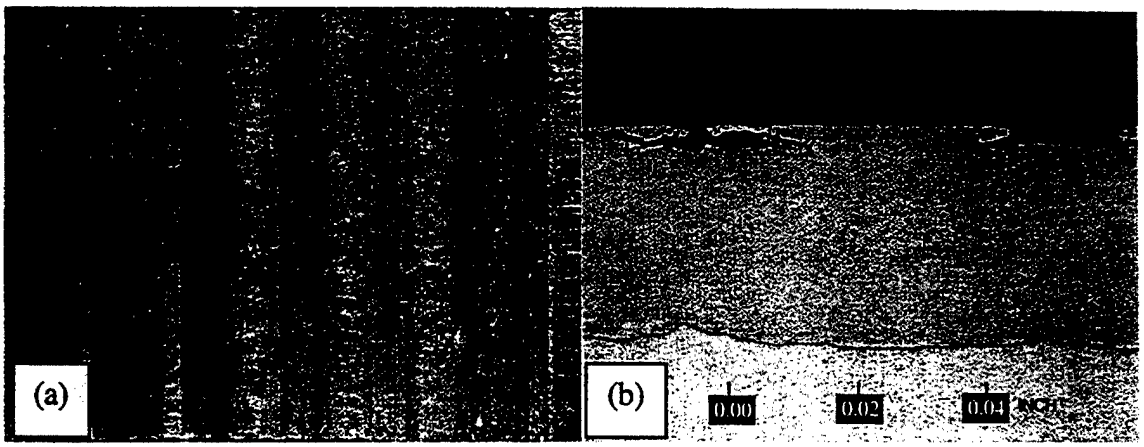

Figure 9. (a) Wear and surface roughening at 28 to 30 inches from RFT, and (b) longitudinal cross-section of Tube C at 50X.

Intermittent mechanical damage can be seen on the lands and in the grooves at the muzzle end (38 to 40 inches from RFT), illustrated in Figure 10. The origin of much of this failure may also lie in degradation at the aforementioned interfacial phase.

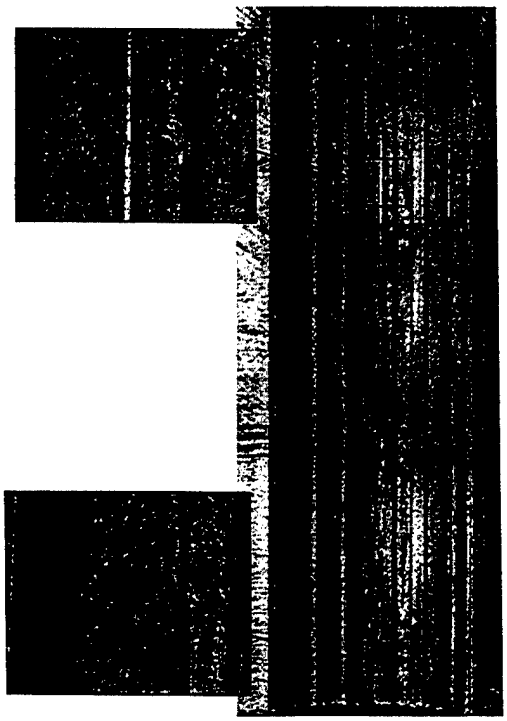

Figure 10. Tube C damage to liner at muzzle.

LINER THICKNESS

Tube A

For Tube A, 360° liner thickness measurements were made of the unfired explosively bonded liner at 5.25, 23, and 40 inches from RFT, using a stereomicroscope. At 5.25 inches, the coating thickness is ~0.038-inch ±3 mils; at 23 inches, the coating thickness is ~0.040-inch ±3 mils; at 40 inches (muzzle end), the coating thickness is ~0.041-inch ±1 mil. The small percentage of deviations in liner thickness around the circumference is inconsequential, considering the thickness of the liner and the fact that the final product is honed to a 25-mm bore diameter.

Tube B

For Tube B, liner thickness measurements were made at 6.5, 10, 14, 20, and 40 inches from RFT in the fired smoothbore specimen. Assuming an initial liner thickness of ~0.040-inch, the final thickness measurements of the liner agree well with the bore gauging measurements taken during testing at Aberdeen Proving Ground (ref 1). Figure 11 illustrates several thickness measurements. See Table 1 for complete coating thickness measurements.

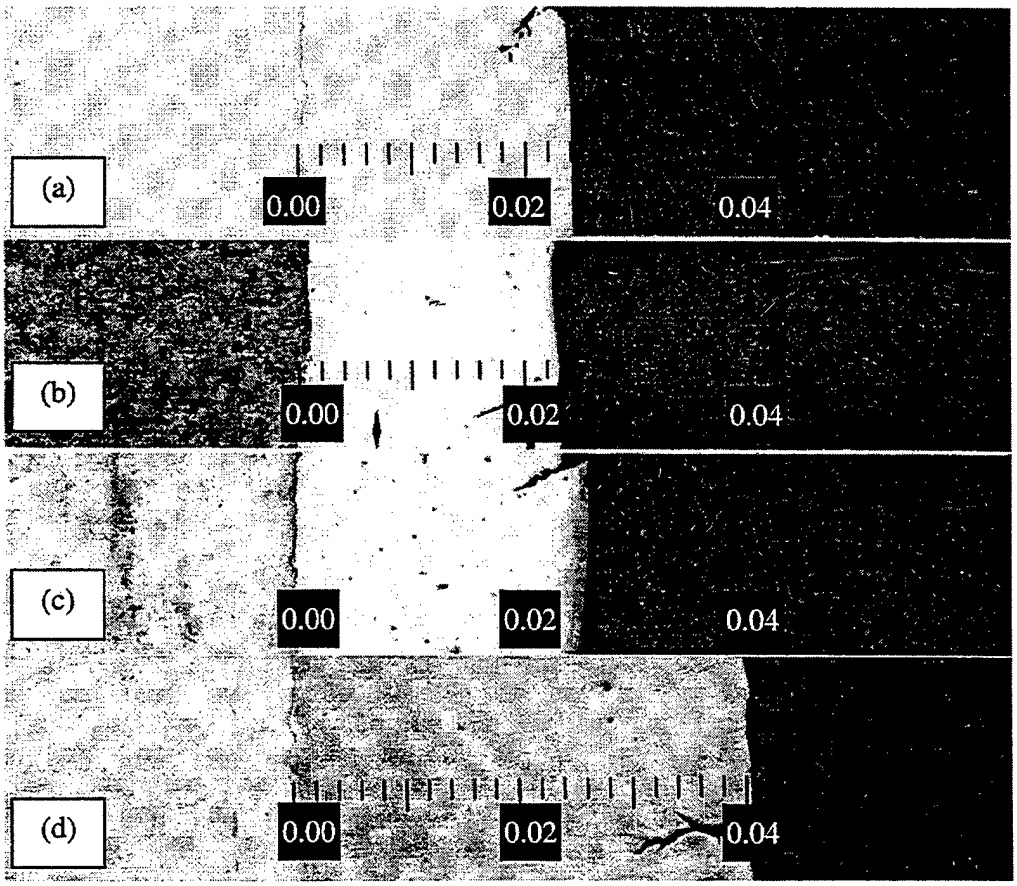

Figure 11. Coating thicknesses of Tube B at (a) 6.5, (b) 10, (c) 14, and (d) 20 inches from RFT.

Tube C

For Tube C, liner thickness measurements were made at 8, 14, 30 and 40 inches from RFT in the fired, no-twist, rifled specimen. At the 8-inch location, the lands were difficult to distinguish from the grooves in the stereomicroscope, as near complete obliteration of the lands had occurred in this location. The liner thickness down bore was much greater than the nominally reported 0.042- and 0.021-inch for land and groove, respectively; but if in fact the liner thickness was indeed 0.060-inch on the lands and 0.037-inch in the grooves, the erosion data compiled at ATC would better correlate to the thickness readings. Figure 12 illustrates several thickness measurements. See Table 1 for complete coating thickness measurements.

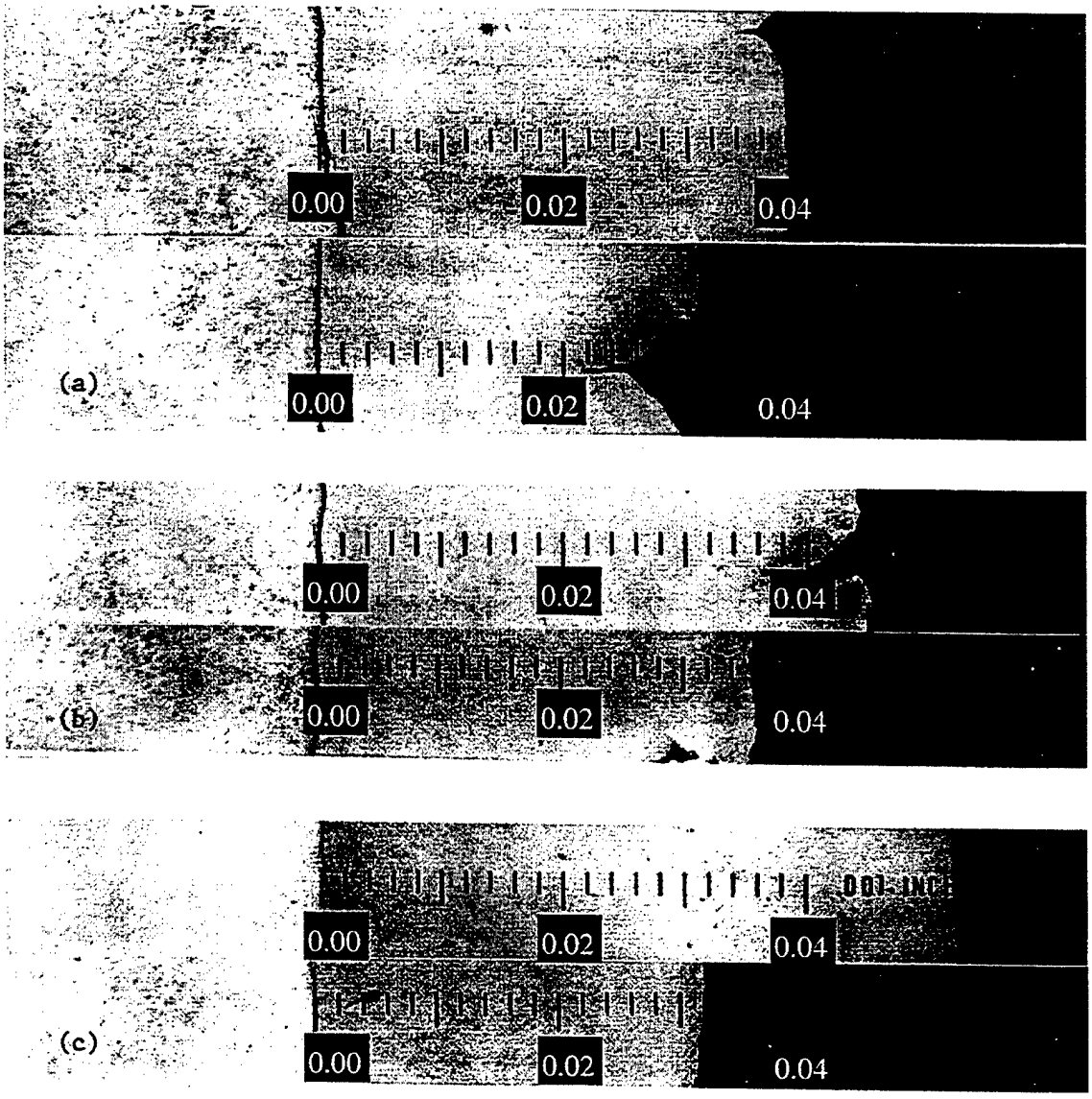

Figure 12. Coating thicknesses of Tube C at (a) 8, (b) 16, and (c) 30 inches from RFT.

Table 1. Liner Thickness Data

Tube B					
Position (Inches from RFT)	**6.5**	**10**	**14**	**20**	**40**
Thickness Average (in.)	0.023	0.015	0.029	0.040	0.041
Tube C					
Position (Inches from RFT)	**8**	**16**	**30**	**40**	
Land Thickness Average (in.)	0.036	0.044	0.055	0.059	
Groove Thickness Average (in.)	0.030	0.034	0.032	0.037	

ADHESION

Samples cut from Tubes A, B, and C were taken and subjected to a modification of the groove adhesion test outlined in ASTM Standard B 571-97, "Standard Test Methods for Adhesion of Metallic Coatings." The modification in the test is a rotation of the tungsten carbide tool bit to facilitate a plowing of material, rather than cutting. This test has been deemed more rigorous for softer coatings by several Benét researchers. All explosively bonded specimens taken from Tubes A, B, and C indicated no signs of adhesive or cohesive failure during the groove test. As was confirmed with these test pieces, the adhesion attainable in explosive bonding tends to be excellent.

MICROSTRUCTURAL ANALYSIS AND MICROHARDNESS

Tube A

Metallographic examination of the unfired specimen revealed a fully dense, defect-free liner material (Figure 13). Along much of the steel/tantalum interface there appeared a hard, brittle intermetallic at all locations. The waveform of the interface is illustrated in Figure 14.

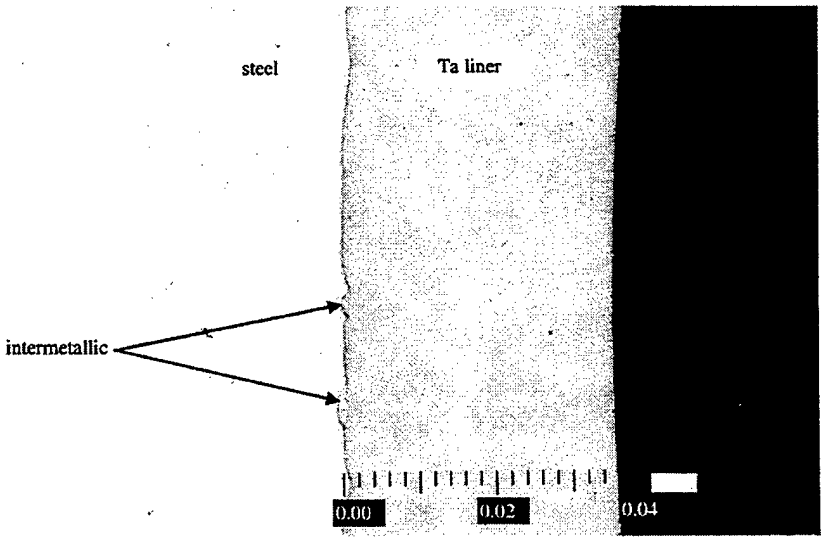

Figure 13. Metallurgical features of Tube A at 50X.

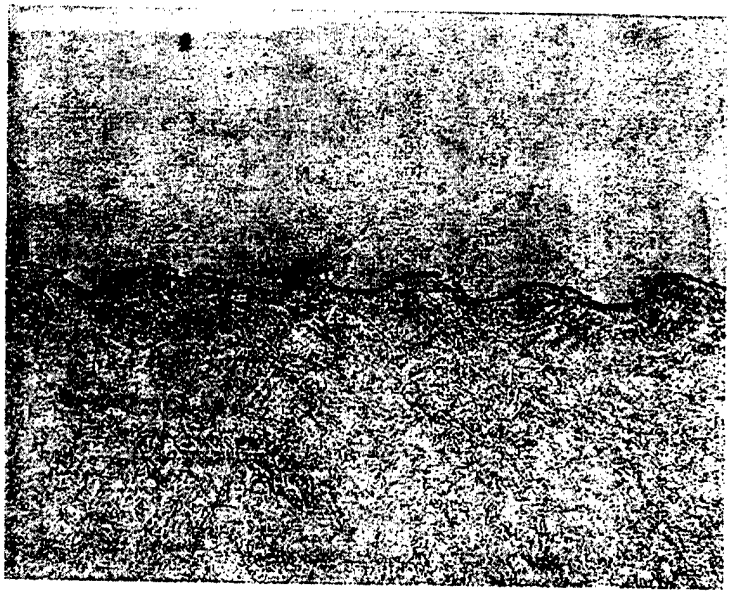

Figure 14. Waveform exhibited by Tube A in axial direction at 500X.

The microhardness of the unfired tube throughout the coating was ~HK_{50} 150. These numbers are consistent with a work-hardened pure tantalum material. Several readings were also taken in the brittle intermetallic present in the coating. The microhardness of the intermetallic was ~HK_{50} 900. Hardness profiles taken in the steel did not indicate the presence of a heat-affected zone. The steel exhibited a tempered martensite structure of ~HK_{50} 365.

Tube B

The liner of Tube B exhibited the same bulk features as Tube A. The liner was dense and defect-free and along much of the interface, a brittle and cracked intermetallic was present. The microhardness of the intermetallic in this tube was also ~HK_{50} 900. An image illustrating the comparative hardness values of the steel, intermetallic, and tantalum liner is given in Figure 15. Besides minor plastic deformation, the steel microstructure appeared relatively unaffected by the explosive bonding process. The one location examined in which the microstructure of the steel was noticeably altered occurred at the 8-inch location (Figure 16b). Although the microstructure is altered, there is no significant hardening or softening of the steel, so the ramifications of this insofar as fatigue life is concerned are unknown.

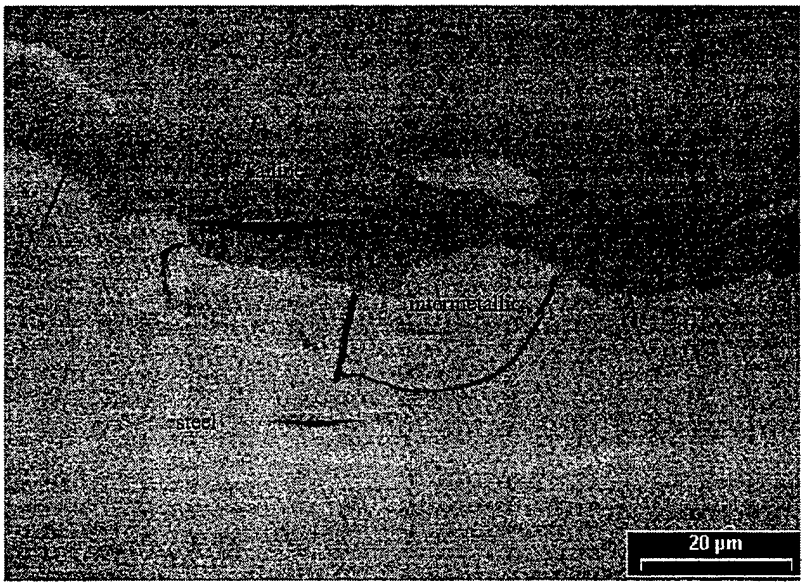

Figure 15. Tube B hardness variations of steel, liner, and intermetallic.

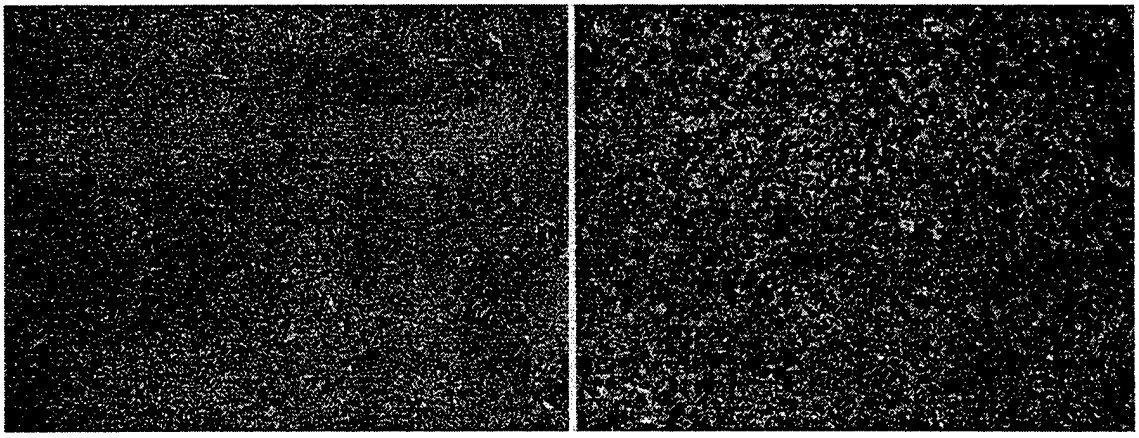

Figure 16. (a) Tempered martensitic structure of Tube B at 500X, and (b) altered interfacial region at 8-inch location at 500X.

Microhardness values taken at various locations are given in Table 2. No significant hardening at the surface of the liner or at the crack tips was found. Considering the oxidation potential of this propellant and the brittle nature of the branched cracks at the surface, this result was initially unexpected. The initial finding gives evidence that hydrogen embrittlement may have played a role in the cracking. This will be discussed further in a later section. Near the surface of the liner in the hottest locations, some softening occurred consistent with high-temperature annealing processes.

Table 2. Microhardness Results

Location	Load (g)	Average Hardness (HK)
Tube B at 8 Inches		
Steel	50	372
Liner Near Interface	50	162
Liner – Bulk	50	134
Liner Near Surface	50	126
Intermetallic	50	962
Tube C at 8 Inches		
Steel	50	365
Liner Near Interface	50	160
Liner – Bulk	50	155
Liner Near Surface	50	132
Intermetallic	50	925
Interphase (30-Inch Location)	10	788

Tube C

The microstructure of the bulk coating of Tube C was dense and defect-free. Again, an intermetallic was present along much of the interface of this specimen exhibiting similar properties as those in Tubes A and B. From metallographic examination, it appears the explosive bonding process was overly energetic at the 30-inch location. Here, a very thick intermetallic (~3 to 5 mils) was present as is illustrated in Figures 17 and 18. Along with this, a shallow heat-affected zone is present in the steel at the interface of the intermetallic.

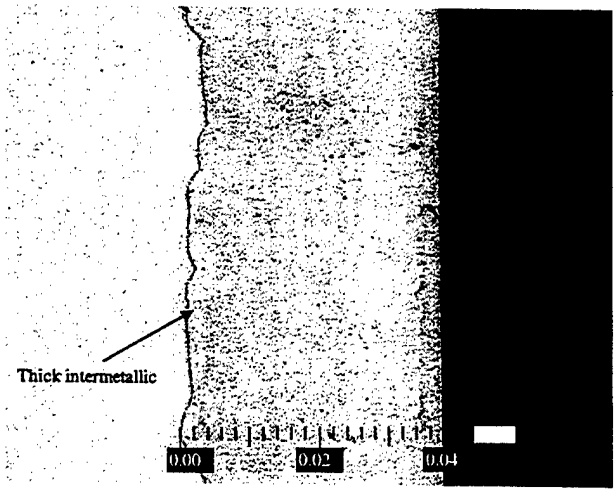

Figure 17. Thick intermetallic of Tube C at 30 inches from RFT at 50X.

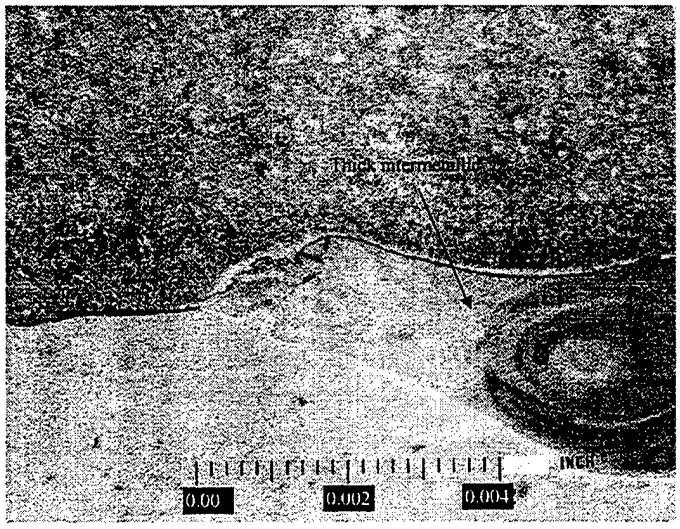

Figure 18. Thick intermetallic and heat-affected zone of Tube C at 30 inches from RFT at 500X.

Besides the intermetallic at the interface, there also appeared to be an intermetallic in the liner itself (Figure 19). This is believed to be due to the dual explosive bonding process in the rifled tube in which two liners were explosively bonded successively, and then the rifling broached out. The appearance of this intermetallic is strange in that it should be a pure tantalum/tantalum bond at this interface. This intermetallic is similarly brittle to the iron/tantalum intermetallic and prone to cracking (Figure 20). The hardness of this intermetallic is ~HK_{50} 800. The composition of this intermetallic was examined using SEM and EDS as discussed below.

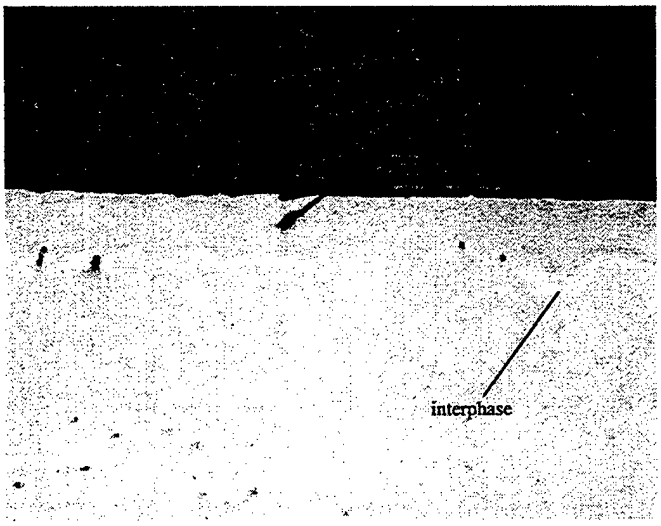

Figure 19. Unidentified phase in rifled liner of Tube C at 150X.

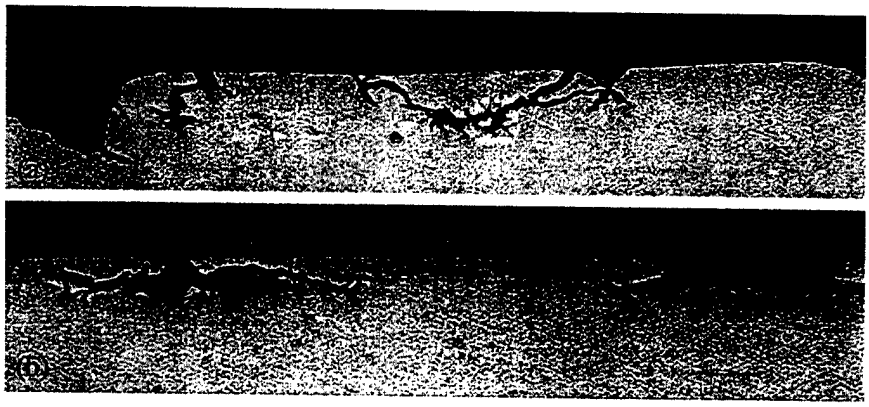

Figure 20. Interphase degradation of Tube C at (a) 8-inch location, and (b) 30-inch location.

SCANNING ELECTRON MICROSCOPY AND ENERGY DISPERSIVE SPECTROSCOPY

Both SEM and EDS were performed on samples taken from Tubes B and C to better observe the nature of the cracking in the coatings, as well as the compositions of the intermetallic phases. The intermetallic present at the interface is an iron/tantalum alloy as illustrated in Figure 21. The compositional analysis attained was expected considering results from past characterization efforts on explosively bonded tantalum (ref 2).

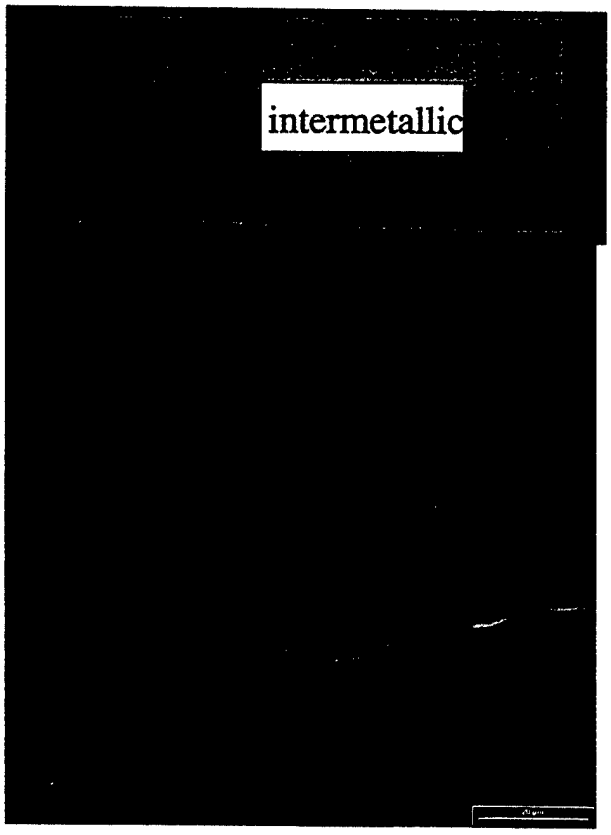

Figure 21. Results of EDS on interfacial intermetallic of Tube C.

Initially, it was postulated that the intermetallic present at the tantalum/tantalum interface in Tube C was possibly an oxide or an unknown pure phase of tantalum formed through explosive bonding. Upon inspection by SEM, it was discovered that the unknown "interphase" was not viewable using standard SEM or compositional electron back-scattering techniques, indicating that it is in all probability, a pure tantalum phase. In conformity with this, the material present cannot be considered an intermetallic and will heretofore be referred to as an interphase. In order to perform EDS on the interphase, a marker taken with an optical microscope was used as illustrated in Figure 22. The EDS results confirm that the phase is indeed pure tantalum. As of yet, the exact phase and crystal structure of this material is unknown. It exhibits microhardness values close to that of the metastable phase β-tantalum (tetragonal), but the presence of this phase is improbable due to the fact that it has only been formed in the past by vapor deposition techniques. Another possibility is the formation of omega (ω) phase (hexagonal) tantalum, which is believed to be a shock-induced phase introduced by high strain rates. This phase has been produced in the past by explosively driven shock-recovery within tantalum cylinders (ref 3).

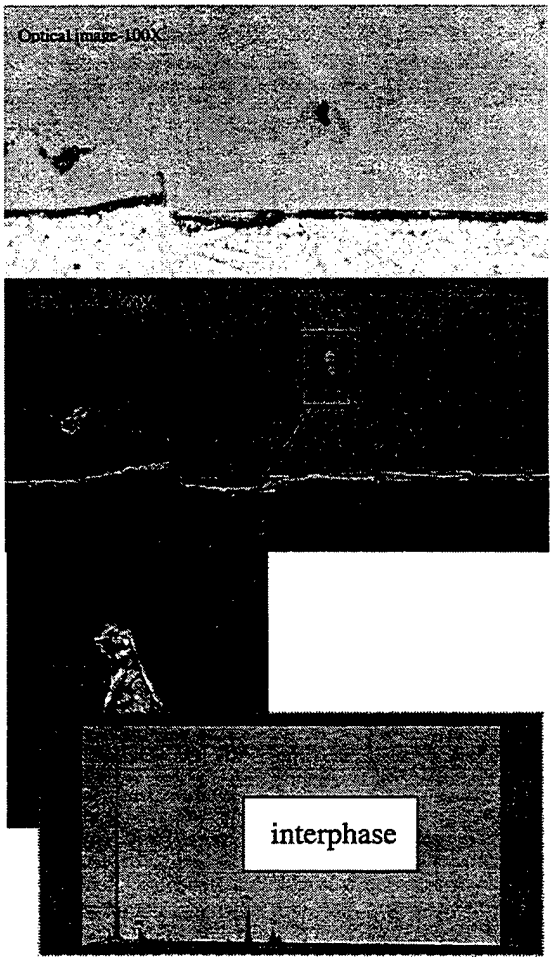

Figure 22. Results of EDS on the interphase developed in Tube C.

Figure 23 illustrates the very brittle nature of the cracking. This is unexpected considering the softness of the liner and the very high ductility of pure tantalum. The occurrence of these branched brittle cracks rules out pure thermal fatigue as the primary mode of cracking and since no significant hardening was discovered around the crack tips, it is unlikely the embrittlement is due purely to oxidation. In hydrogen embrittlement of pure tantalum, significant hardening is generally not observed. This leads us to believe the embrittlement of the coating at the surface may be due to hydrogen absorption. To confirm this, residual hydrogen concentration analyses were conducted and will be discussed later.

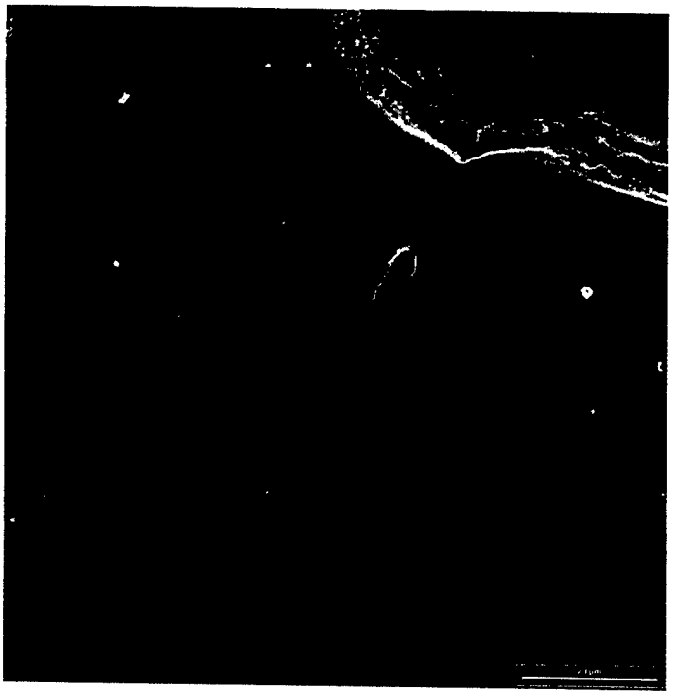

Figure 23. Brittle branched cracking at surface of the Tube C tantalum liner at 1100X.

In addition, Figure 23 illustrates a gray layer observed on the surface. Based on EDS results, this layer appears to be a tantalum oxide (Figure 24). This is further supported by the WDS results described next.

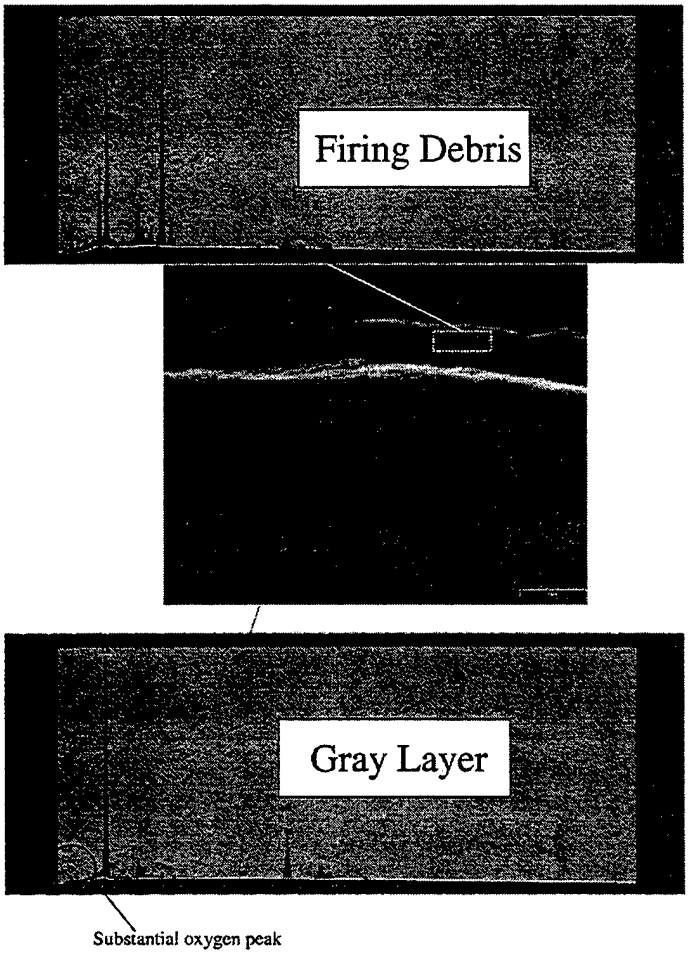

Figure 24. Results of EDS on surface layer of the Tube C tantalum liner.
The substantial oxygen peak observed indicates the presence of a surface oxide.

WAVELENGTH DISPERSIVE SPECTROSCOPY

Wavelength dispersive spectroscopy was conducted on sections taken from Tube B to determine the nature and composition of the tantalum liner surface. The results indicate that there is a tantalum oxide on the surface. The data is semi-quantitative and comparing the results taken from the surface of the explosively bonded tantalum (Appendix A) and those taken from a tantalum oxide chip (Appendix B), gives conclusive evidence of the presence of an oxide. Results are given in values of wt. %. Note the comparable findings with concern to tantalum and oxygen.

HYDROGEN ANALYSIS

A LECO hydrogen determinator was implemented to determine the concentration of hydrogen in the explosively bonded coatings. The liner was removed from the steel substrate through the use of a tungsten carbide too bit. As was expected, the coating exhibited a high content of hydrogen in the coating. The results are listed in Table 3. The fact that a higher residual hydrogen concentration was measured for Tube B is logical considering that the smoothbore gun tube endured 1385 rounds, whereas the rifled bore Tube C endured only 600.

TABLE 3. Hydrogen Concentration in Liner

Sample	Mass (g)	Wppm H	Average wppm H
Tube B at 18 Inches from RFT #1	0.1970	159.60	
#2	0.2300	147.10	153.40
Tube C at 14 Inches from RFT #1	0.2203	118.50	
#2	0.2416	121.00	119.80
Tube A	0.2436	32.04	32.04

PULSED LASER HEATING

To determine the thermomechanical integrity of the liners and if the residual hydrogen concentration of Tube B was sufficient to induce hydrogen embrittlement, pulsed laser heating was conducted on samples taken from the fired Tube B and the unfired Tube A. Also, in order to examine the thermomechanical integrity of the interface, the samples were ground to a thickness of ~5 to 10 mils.

Experimental Approach

Two specimens were prepared for pulsed laser heating experiments. Sample A was taken from the unfired Tube A, and Sample B was taken from Tube B. The specimens were cut from ring sections of each tube at locations 30 inches from RFT for Tube A, and 8 inches from RFT for Tube B. The specimen from Tube A was cut to an approximate size of 8x7x2.5-mm, and the specimen from Tube B was cut to an approximate size of 6x7x2.5-mm. Each was ground flat to ensure a coating thickness that ranged from 5 to 10 mils. Grinding began with 240 grit and ended with 600 grit silicon carbide paper.

In the pulsed laser heating experiments, radiation from a neodymium-doped yttrium aluminum garnet (Nd:YAG) laser was delivered to each test specimen surface. The wavelength of the radiation was 1064 nanometers, the pulse duration was 5-ms (at half maximum), and the spot diameter at the specimen surface was 2.6-mm for both spots on Tube A. For Tube B, spot 1 diameter = 2.6-mm and spot 2 = 3.4-mm. Since the depth of the high temperatures and high thermal gradients is typically less than 0.2-mm, the heat flow for most of the heated area is approximately one-dimensional and normal to the surface, as it would be on an actual gun bore surface.

A significant portion of the laser energy may be reflected rather than absorbed, depending on surface roughness and oxidation, both of which may change during heating. Therefore, the absorbed energy was measured calorimetrically, using a thermocouple spot-welded to the opposite face of the specimen to measure the specimen's overall temperature rise. The need to measure the overall temperature rise limited the size of the specimens to the dimensions given earlier. All pulse energy values quoted are for energy absorbed rather than incident.

Both specimens were laser pulsed in two separate locations with average energy densities ranging from 0.90 to 1.10 J/mm^2, as indicated below. Note: 1.0 J/mm^2 is representative of the thermal input into cannon bores with conventional high-temperature propellants.

Following laser pulsing, the specimens were cross-sectioned, mounted, and then mechanically polished using silicon carbide sandpaper, followed by a final polish with 7 μm diamond paste and a slurry of 0.05 μm alumina oxide powder and water. All imaging was performed using a 1LM21W Nikon/Lasertech Laser Scanning Confocal Microscope System in the two-dimensional optical mode.

Experimental Results

Sample A from Tube A: General Observations

Etching revealed banding parallel to the tube axis throughout the steel substrate of Sample A, as shown in the cross-section of Figure 25. There are many occurrences of inclusions oriented along the bands. These features reflect the quality of material used for the manufacture of this gun tube.

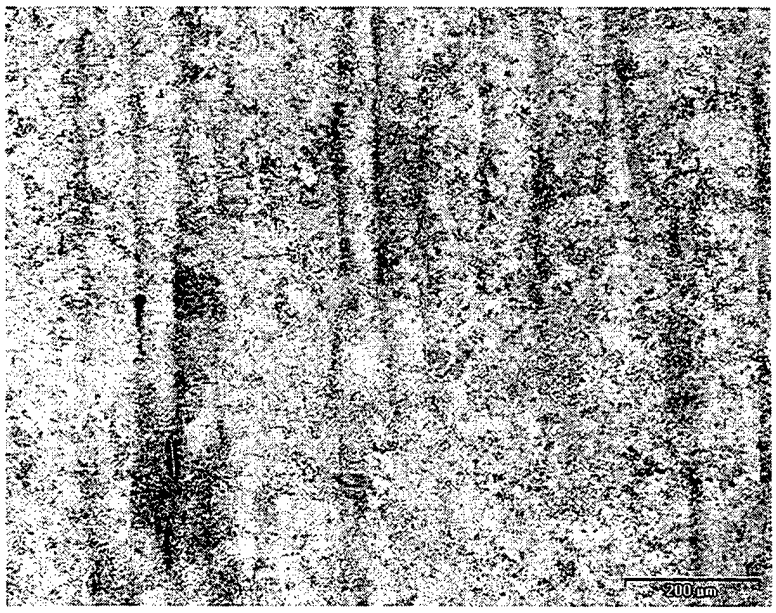

Figure 25. Substrate steel of unfired explosively bonded tantalum-coated gun tube at magnification 200X. This cross-section is perpendicular to the bore and parallel to the tube axis.

Also observed was the formation of an intermetallic phase found at random locations throughout the irregular explosively bonded tantalum/steel interface, as shown in Figure 26. As no heat-affected zone is seen adjacent to these regions, this intermetallic phase was produced without high heating. These results are consistent with the cold welding process attributed to explosive bonding.

Figure 26: Explosively bonded tantalum/steel interface of Sample A at magnification 2000X.

Laser Pulsing of Sample A, Tube A, Spot 1

Sample A was laser pulsed in two locations. Spot 1 was laser heated with 23 pulses, the first 3 at or below 0.86 J/mm^2 and the next 20 at an average of 1.09 J/mm^2. (Because it is impossible to predict the percent of energy that will be absorbed, a low-incident energy was selected for the first few pulses in order to avoid overshooting and delivering more energy than desired.) Figure 27 shows a region of the surface near the center of spot 1 following the 23 pulses.

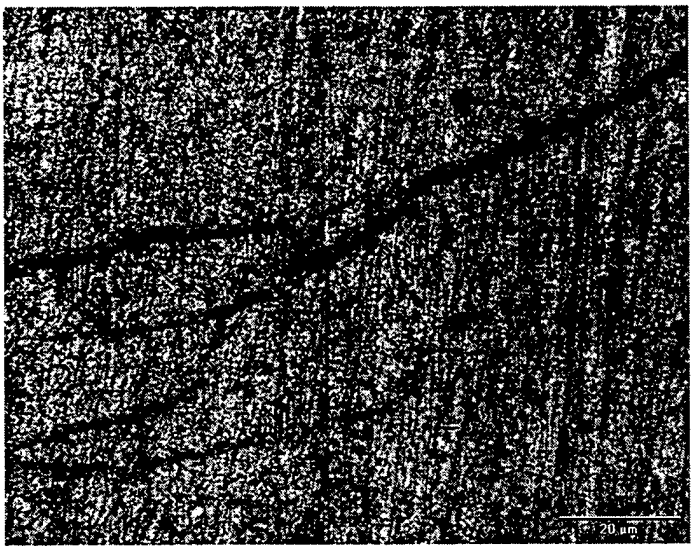

Figure 27. Laser pulsed region of unfired explosively bonded tantalum coating at magnification 2000X.

Staining throughout the pulsed region indicates that an oxide layer formed during heating. It was observed that there is a tendency for rapid oxidation of the explosively bonded tantalum during pulsing in air at ambient conditions. The surface cracks shown here are representative of those found throughout spot 1, with widths ranging from approximately 0.5 to 3.0 μm.

Figure 28 shows the cross-section of spot 1 taken at a magnification 200X. This image illustrates cracking of the brittle intermetallic phase, along with the formation of a small heat-affected zone in the steel adjacent to the interface. Coating thickness is approximately 210 μm within the pulsed region.

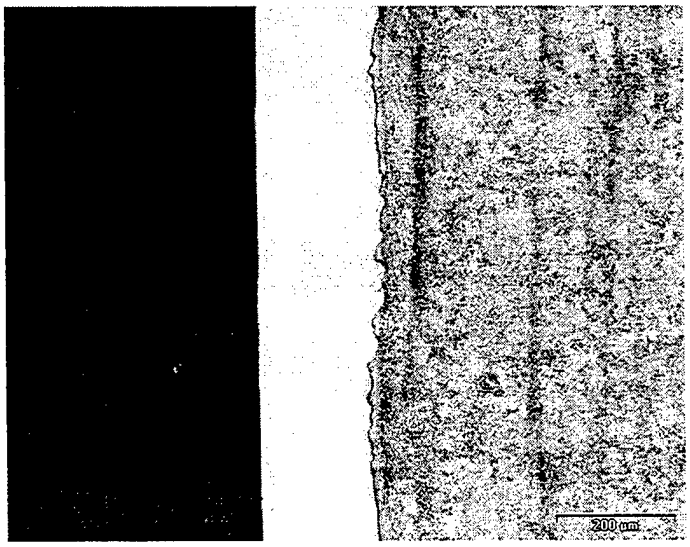

Figure 28. Laser pulsed spot 1 at magnification 200X.

While fine cracking of the intermetallic phase was seen throughout some locations along the interface, larger cracks were found in the intermetallic phase within the laser pulsed regions. Figure 29 shows the interface of spot 1 at increased magnification.

Figure 29. Effects of laser pulsing spot 1 at magnification 1200X.

Here the heat-affected zone is seen to extend approximately 8 to 15 μm into the steel substrate. It is nonuniform, and appears along the waveform where the steel rises higher into the coating. Figure 30 shows a 2- to 3-μm thick oxide layer that has formed on the tantalum surface. Within the cross-sections of the laser-heated spots, no surface cracks have progressed through the oxide layer, suggesting that the explosively bonded tantalum is resistant to crack propagation from thermal shock.

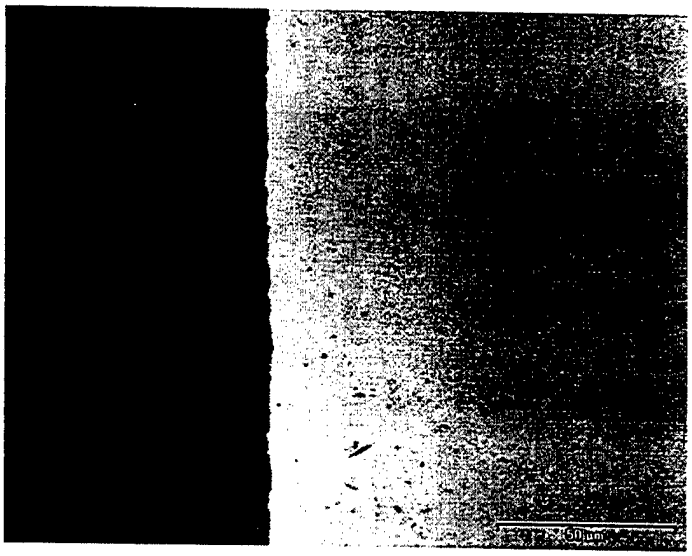

Figure 30. Surface oxide layer from laser pulsing spot 1 at magnification 2000X.

Laser Pulsing of Sample A, Tube A, Spot 2

As previously stated, Sample A was laser pulsed in two locations. Spot 2 was similarly heated with 23 pulses, the first 3 at or below 0.81 J/mm^2 and the last 20 at an average of 1.09 J/mm^2. Figure 31 shows a region of the surface near the center of spot 2 following the 23 pulses.

Figure 31. Laser pulsed region of Tube A liner at magnification 2000X.

The surface cracks shown here are similar to those found on spot 1, with widths ranging from approximately 0.5 to 3.0 μm. Again, staining throughout the pulsed region indicates that an oxide layer had formed during heating. Figure 32 shows the cross-section of spot 2 taken at magnification 200X.

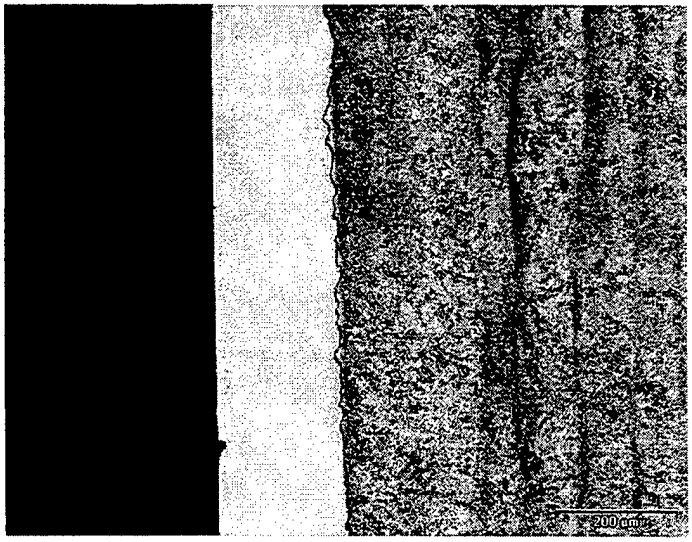

Figure 32. Laser pulsed spot 2 at magnification 200X.

Figure 32 also illustrates once again, the highly irregular interface with small regions of intermetallic phase present. A heat-affected zone is also seen in the steel adjacent to the interface. Coating thickness is approximately 210 μm within the pulsed region. Figure 33 shows this interface at increased magnification.

Figure 33. Effects of laser pulsing spot 2 at magnification 1200X.

Here the heat-affected zone is seen to extend approximately 8 to 10 μm into the steel substrate. It is nonuniform and appears where the steel rises higher into the coating. Figure 34 shows a 2- to 3-μm thick oxide layer that has formed on the tantalum surface. Within the region shown, one surface crack has progressed through the oxide layer.

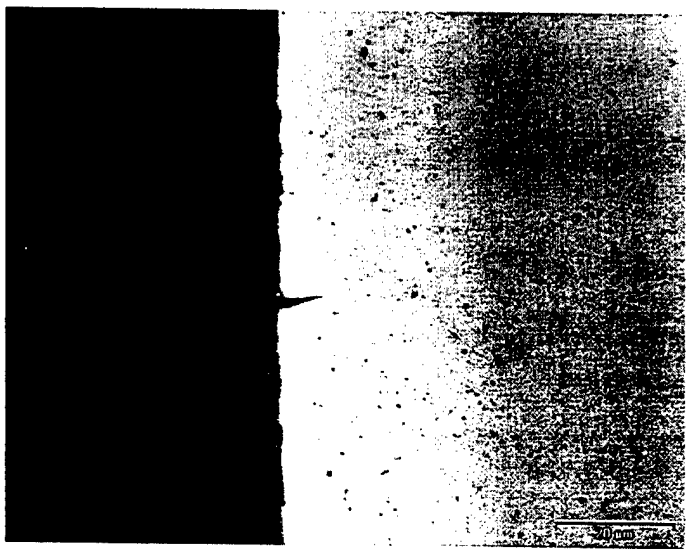

Figure 34. Surface oxide layer from laser pulsing spot 2 at magnification 2000X.

Sample B from Tube B: General Observations

Similar to the unfired specimen, etching revealed banding parallel to the tube axis and inclusions throughout the steel substrate of Sample B, as shown in the cross-section of Figure 35.

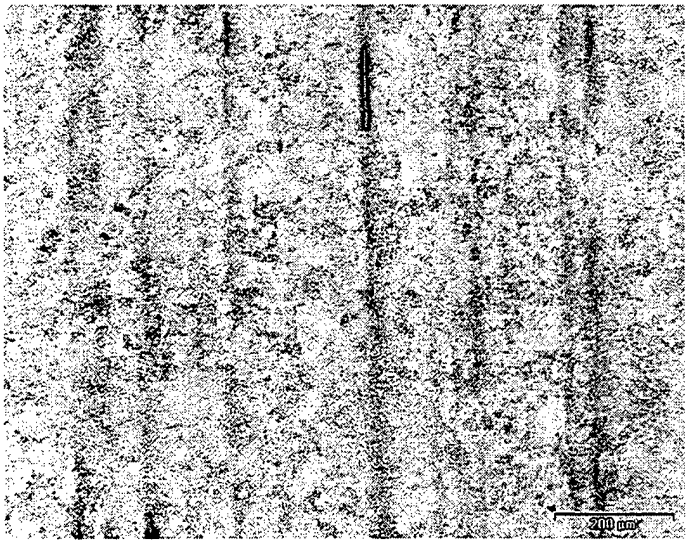

Figure 35. Substrate steel of fired explosively bonded tantalum-coated gun tube at magnification 200X. This cross-section is perpendicular to the bore and parallel to the tube axis.

Laser Pulsing of Sample B, Tube B, Spot 1

Sample B was laser pulsed in two locations. Spot 1 was laser heated with 22 pulses, the first 2 at or below 0.95 J/mm^2 and the next 20 at an average of 1.10 J/mm^2. Figure 36 shows a region of the surface near the center of spot 1 following the 22 pulses.

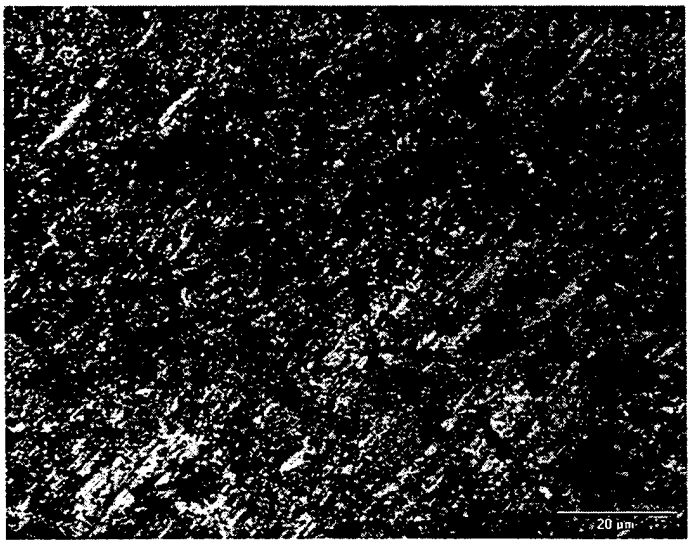

Figure 36. Laser pulsed region of unfired explosively bonded tantalum coating at magnification 2000X.

Staining throughout the pulsed region indicates that an oxide layer had formed during heating. Unlike the unfired explosively bonded coating, here the surface is found to consist of several ledge-like features. While no surface cracks are shown within this region, inspection of the cross-section in Figure 37 shows that minor surface cracking occurred.

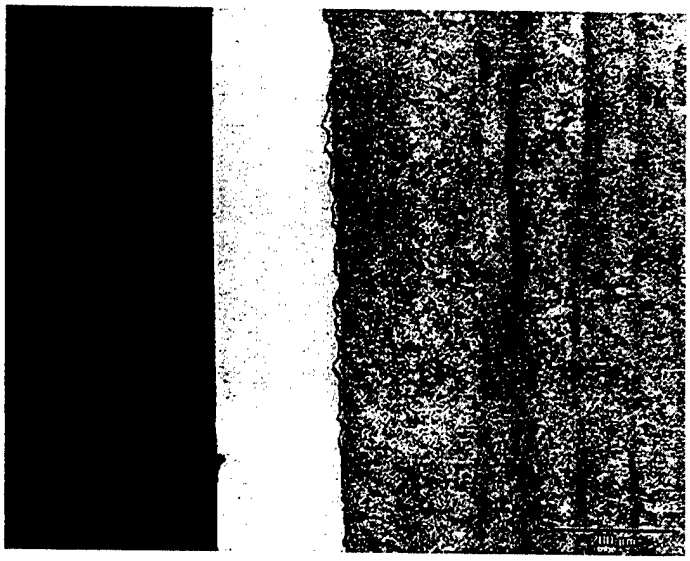

Figure 37. Laser pulsed spot 1 at magnification 200X.

Figure 37 also shows the formation of a heat-affected zone adjacent to the irregular explosively bonded tantalum/steel interface. Coating thickness is approximately 190 μm. Figure 38 shows the interface at increased magnification. Here the heat-affected zone is seen to be fairly uniform, and extends approximately 10 to 15 μm into the steel substrate.

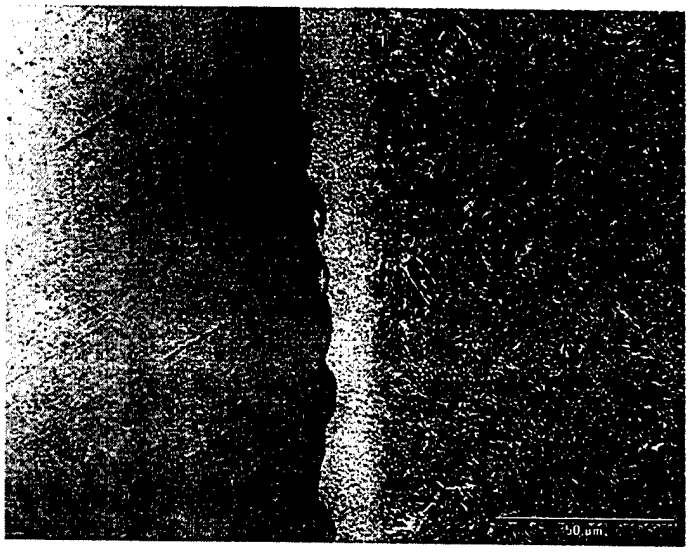

Figure 38. Effects of laser pulsing spot 1 at magnification 1200X.

Figure 39 shows a 2- to 3-μm thick oxide layer that has formed at the tantalum surface. Here a surface crack is shown that has progressed through the oxide layer into the explosively bonded tantalum, and has propagated about 9 μm into the coating.

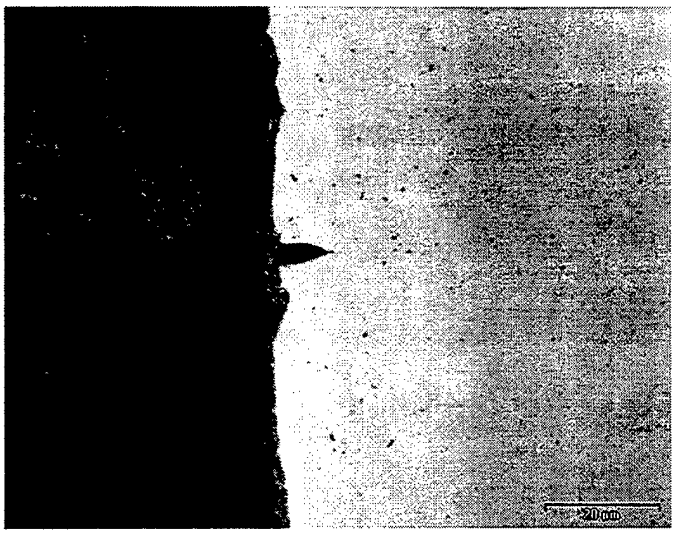

Figure 39. Surface oxide layer from laser pulsing spot 1 at magnification 2000X.

Laser Pulsing of Sample B, Tube B, Spot 2

As previously stated, Sample B was laser pulsed in two locations. Spot 2 was laser heated with 23 pulses, the first 3 at or below 0.72 J/mm^2 and the next 20 at an average of 0.91 J/mm^2. Figure 40 shows a region of the surface near the center of spot 2 following the 23 pulses. Similar to spot 1, this surface is seen to consist of several ledge-like features. While no surface cracks were seen within this region, inspection of the cross-section of this specimen shows that minor surface cracking did occur.

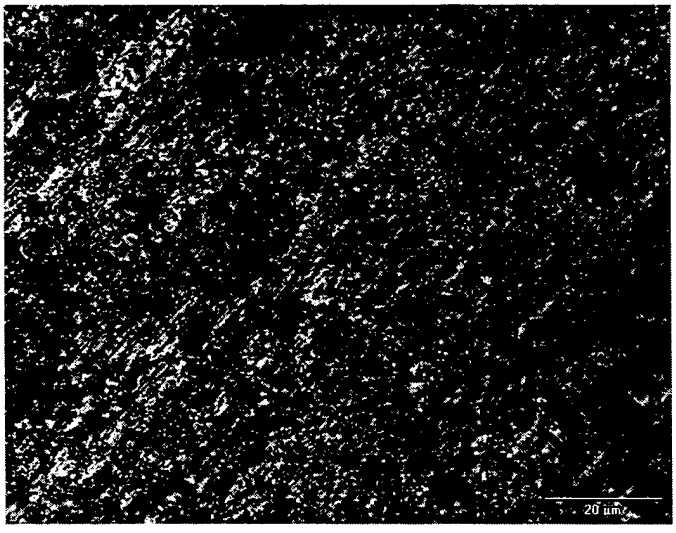

Figure 40. Laser pulsed region of unfired explosively bonded tantalum coating at magnification 2000X.

Figure 41 shows minimal formation of a heat-affected zone in the steel adjacent to the interface. This is attributed to both the lower pulse energy used at this location and an increased thickness of the explosively bonded coating as compared to spot 1. Here the average coating thickness is 230 μm.

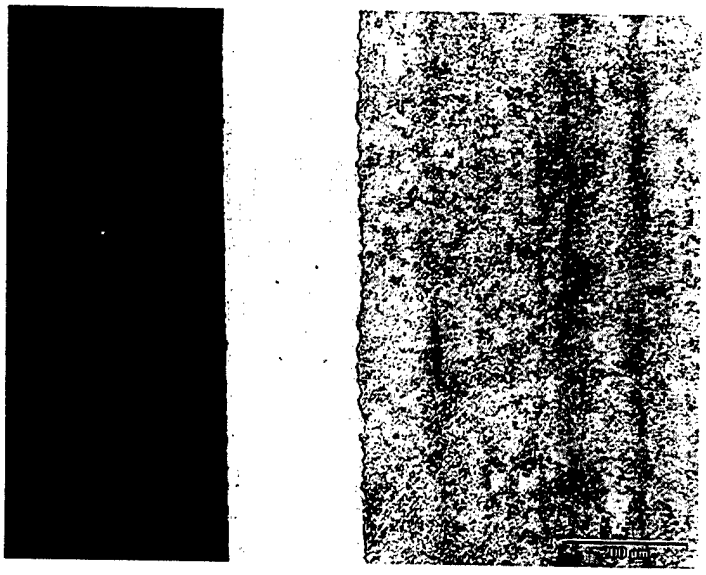

Figure 41: Cross-section of spot 2 taken at magnification 200X.

Figure 42 shows this interface at increased magnification. Here the small heat-affected zone is seen to extend approximately 3 to 4 μm into the steel substrate.

Figure 42: Effects of laser pulsing spot 1 at magnification 1200X.

Figure 43 shows a 2- to 3-μm thick oxide layer that has formed at the tantalum surface. Within this region, one surface crack has progressed through the oxide layer.

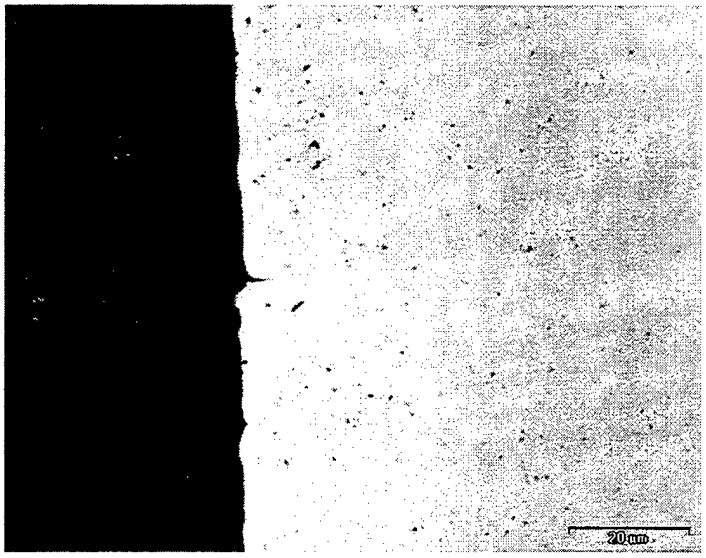

Figure 43. Surface oxide layer from laser pulsing spot 2 at magnification 2000X.

Comments

Results from Benet Laboratories pulsed laser heating studies of explosively bonded tantalum liners indicate that this material has good resistance to thermal shock and to thermal fatigue. Both fired and unfired coatings show excellent adhesion to steel substrates. Intermetallic phase formation was found at random locations throughout the irregular coating/steel interface and is attributed to the explosive bonding process. Fine cracking of the intermetallic phase was often seen. In the laser pulsed regions, by contrast, relatively large cracks tended to form in the intermetallic phases.

Following pulsed laser heating, cracking was more perceptible in Tube B as opposed to Tube A. For the unfired tube, cracking was not expected since very little hydrogen was present. The outcome was uncertain for the fired tube considering the residual hydrogen content was relatively high (~150 wppm). Although some surface cracking did occur, the nature of the cracking was not brittle and branched as that seen in the characterized fired tubes. It is possible that a hydrogen gradient was present in the coating and the overall concentration was lower near the interface. In addition, during gun firing, the local concentration of hydrogen would be much higher at the crack tip and thus embrittlement would be much more likely.

DISCUSSION

Tube B

The basic erosion mechanism observed in the fired smoothbore tube appears to be a process involving several steps (ref 4). Due to the high flame temperatures and reactive nature of the "original" M919 propellant in which both reducing (H_2) and oxidizing constituents are present (ref 5), along with the lack of high-temperature oxidation resistance of pure tantalum, the predominant mechanism causing the initial uniform erosion of the liner may have been thermochemical in nature. One proposed mechanism is the persistent formation and subsequent removal of a surface oxide. This mechanism is supported by several facts. First, pulsed laser heating at high enough energy on sputtered tantalum has led to the formation of a surface oxide scale in laboratory air. Also, x-ray fluorescence and EDS examination of the surface of the fired tube give evidence of an oxide present. Of course, at the sustained temperatures of the firing test, particularly in the rapid-fire mode bursts, a type of thermomechanical erosion may also have played an important role. The liner will have experienced significant softening and, in turn, the potential for swaging and sloughing off of the coating by the sweeping gases is increased. This mechanism has been exhibited in past tantalum coatings (ref 6). It is likely that the erosion process is a combination of both thermomechanical and thermochemical processes.

Following sufficient uniform erosion of the liner, the propensity for blow-by of the hot gases due to poor obturation increases. This stage of the erosion process is illustrated by the gas-wash grooves shown in Figures 3 and 4. The inset in Figure 3 is an example of a gas-wash groove following along the heat-check cracking caused by hydrogen embrittlement. The heat-check cracks act as a conduit for the axially oriented gas-wash grooves, thus increasing the speed of this erosion process. Figure 44 is a cross-section taken at the 10-inch from RFT location, and illustrates the severity and dominance of the hot gas erosion at this stage. The final stage of the erosion process exhibited in this tube is in full erosion of the liner at an axially oriented groove and subsequent rapid erosion in the steel as is illustrated in Figure 45.

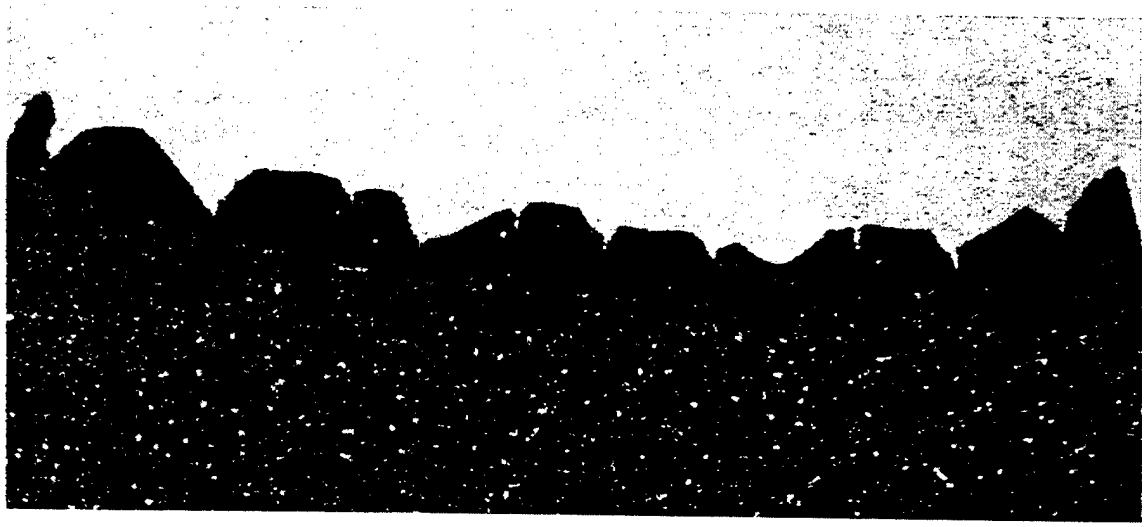

Figure 44. Stereomicrograph of severe gas erosion in Tube B at 10 inches from RFT at 10X.

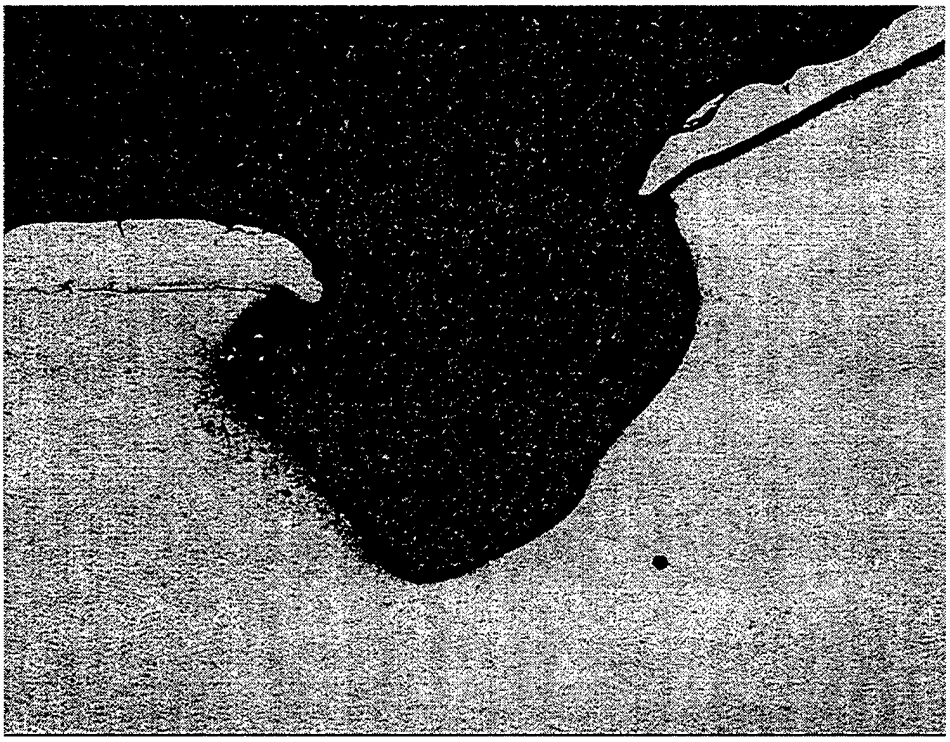

Figure 45. Severe erosion of underlying steel in Tube B at 8 inches from RFT at 15X.

Tube C

The main area of concern in the erosion of the no-twist rifled Tube C is the obliteration and overall damage to the lands extending down bore to at least 16 inches from RFT. Considering that the gun bore consisted of a *no-twist* rifling alignment, the mechanical stresses on the liner were not as severe as would be the case in a true Bushmaster gun tube.

The overall erosion characteristics and cracking of Tube C are similar to that of Tube B with the exception of failure of the liner at the interphase tantalum formed by the dual-explosive bonding process. The presence of this phase at an interface near the surface of the liner may lead to extensive premature liner spallation of the lands during firing.

CONCLUSIONS/RECOMMENDATIONS

Explosively bonded tantalum was applied to three modified, previously fired, Bushmaster barrels. Prior to the explosive bonding process, each barrel had been machined to remove all of the existing rifling and any erosion from prior firing. All the tubes had been shortened to approximately 40 inches, since it was felt that the explosive bonding process would rupture the forward, thinner-walled portions of the barrels. Tubes A and B were cladded and machined to a smoothbore 25-mm configuration, while Tube C was cladded and machined to a straight-rifled (no-twist) 25-mm configuration.

The explosive bonding technology demonstrated here was shown to have made significant improvement over explosively bonded cylindrical coupons provided to Benét Laboratories during 2000. Adhesion of the tantalum to the substrate is superior and though an undesired intermetallic still exists between the tantalum and the substrate, its overall presence has been reduced from past specimens characterized. A few technical concerns regarding the liner material itself include the softness of the tantalum and its chemical reactivity as discussed in the previous section. It would be beneficial to explore the cladding of tantalum alloy liners with alloy additions aimed specifically at increasing strength, wear resistance, and corrosion resistance. Alloying additions that may be useful include molybdenum and tungsten. Both molybdenum and tungsten act as fairly potent hardening agents of tantalum. In addition to increased hardness and strength, it has been shown that molybdenum increases the ability of tantalum to resist hydrogen embrittlement (ref 7). While alloying would be beneficial, the degree of strengthening must be closely monitored considering that for successful explosive bonding, a material must have a percent elongation of 16 to 20 (ref 8). This limitation still leaves room for improvement in mechanical properties. For instance, commercially pure electron beam melted tantalum has an elongation of ~30 to 40% and a yield strength of ~5 Ksi at 1000°C, while Ta-10W has an elongation of ~25% (within limits of explosive bonding) and a yield strength of ~30 Ksi at 1000°C (ref 9).

Aside from pure materials issues, from an armaments perspective, it is important to understand that extrapolations of this test data to fielded weapon system performance may be premature. The test assets used in this research demonstration (smoothbore and no-twist rifled 25-mm barrels) do not represent any fielded system at this time. The current fielded 25-mm Bushmaster barrel employs gain-twist rifling that offers a harsher mechanical environment than no-twist rifling or a smoothbore design.

In summary, the characterization results indicate a significant improvement has been made in the explosive bonding process during the last few years. As evidenced by the increase in barrel life over standard nitrided Bushmasters, this process continues to demonstrate great potential as a wear and erosion-resistant coating deposition process for protecting the bores of cannon barrels. Additional work should be pursued in the area of wear and erosion mitigation technologies, and the work described here is certainly worthy of continuation to this end. Further work will be necessary to perfect the explosive bonding process, apply and test it on existing weapon platforms, as well as address the significant full-scale manufacturing issues.

REFERENCES

1. Hubbard, L.M., "Final Report for the M242 25-mm Cannon Erosion Investigation," S-51323, U.S. Army Aberdeen Test Center, Aberdeen Proving Ground, MD, April 2001.

2. Vigilante, G., Cote, P., Sage, T., Lee, S., Kendall, G., and Audino, M., "Characterization of Tantalum Liners Applied to 25-mm and 120-mm Cannon Bore Sections Via Explosive Bonding," ARDEC Technical Report ARCCB-TR-01003, Benét Laboratories, Watervliet, NY, February, 2001.

3. Hsiung L.M., and Lassila, D.H., "Shock Induced Omega Phase in Tantalum," *Scripta Materiala*, Vol. 38, No. 9, 1998, pp. 1371-1376.

4. Underwood, J., private communication, Benét Laboratories, Watervliet, NY, October 2001.

5. Sopok, S., private communication, Benét Laboratories, Watervliet, NY, October 2001.

6. Ahmad, I., "The Problem of Gun Barrel Erosion: An Overview," *Progress in Astronautics and Aeronautics*, Vol. 109, AIAA, Washington, DC, 1988.

7. Gypen, L.A., Brabers, M., and Deruyttere, A., "Corrosion Resistance of Tantalum Based Alloys. Elimination of Hydrogen Embrittlement in Tantalum by Substitutional Alloying," *Werkstoffe und Korrosion*, Vol. 35, 1984, pp. 37-46.

8. Vigilante, G., private communication, Benét Laboratories, Watervliet, NY, October 2001.

9. *Advanced Materials and Processes*, Vol. 156, No. 6, 1999, pp. 125-126.

APPENDIX A. X-RAY FLUORESCENCE DATA FOR TUBE B

DEPARTMENT OF THE ARMY - BENET LABS - WATERVLIET ARSENAL
SRS 3000 Siemens SemiQuant Interactive Evaluation Program 19-Oct-2001 11:56
Sample Id. : B_EBTA_8_8.75
-- Results -- -- XRF Concentration -- Measured on 30-Sep-2001 11:33

Ta	52.8	%	XRF		41.7	þ	0.24	%	Ta LA1
O	22.0	%	XRF		17.4	þ	2.39	%	O KA1
C	15.7	%	XRF		12.4	þ	8.16	%	C KA1
K	3.15	%	XRF		2.49	þ	0.076	%	K KA1
Fe	1.62	%	XRF		1.28	þ	0.048	%	Fe KA1
Na	1.24	%	XRF		0.98	þ	0.245	%	Na KA1
Si	0.491	%	XRF		0.388	þ	0.0528	%	Si KA1
Zn	0.479	%	XRF		0.378	þ	0.0199	%	Zn KA1
S	0.473	%	XRF		0.373	þ	0.0284	%	S KA1
Ba	0.448	%	XRF		0.354	þ	0.0582	%	Ba LA1
Al	0.213	%	XRF		0.169	þ	0.0270	%	Al KA1
Cl	0.204	%	XRF		0.161	þ	0.0285	%	Cl KA1
Er	0.145	%	XRF	?	0.115	þ	0.0587	%	Er LB1
Ca	0.124	%	XRF		0.098	þ	0.0254	%	Ca KA1
Rh	0.120	%	XRF		0.095	þ	0.0404	%	Rh KA1F
Te	0.115	%	XRF		0.091	þ	0.0622	%	Te LA1
Mg	0.0925	%	XRF		0.0731	þ	0.04898	%	Mg KA1
Nd	0.0903	%	XRF		0.0713	þ	0.04171	%	Nd LA1
P	0.0808	%	XRF		0.0639	þ	0.01992	%	P KA1
Sn	0.0751	%	XRF		0.0593	þ	0.04914	%	Sn LA1
Pb	0.0730	%	XRF		0.0576	þ	0.03158	%	Pb LB1
Sm	0.0659	%	XRF		0.0521	þ	0.04437	%	Sm LA1
Cr	0.0620	%	XRF		0.0490	þ	0.01792	%	Cr KA1
Th	0.0420	%	XRF		0.0332	þ	0.02179	%	Th LB1
Mn	0.0345	%	XRF		0.0273	þ	0.01758	%	Mn KA1
V	0.0338	%	XRF		0.0267	þ	0.01325	%	V KA1
Cd	0.0337	%	XRF			<	0.05521	%	Cd KA1F
Ni	0.0278	%	XRF		0.0219	þ	0.01570	%	Ni KA1
Ti	0.0160	%	XRF		0.0126	þ	0.01252	%	Ti KA1
Ga	0		XRF			<	0.01922	%	Ga KA1
Ge	0		XRF		0.1241	þ	0.01884	%	Ge KA1
As	0		XRF			<	0.07319	%	As KB1
Se	0		XRF	?	0.2605	þ	0.04804	%	Se KA1
Br	0		XRF			<	0.02821	%	Br KA1
Rb	0		XRF			<	0.04478	%	Rb KA1
Sr	0		XRF			<	0.00784	%	Sr KA1
Y	0		XRF			<	0.01203	%	Y KA1
Zr	0		XRF			<	0.00859	%	Zr KA1
Nb	0		XRF			<	0.00735	%	Nb KA1
Mo	0		XRF			<	0.00708	%	Mo KA1
Ru	0		XRF			<	0.02314	%	Ru KA1F
Pd	0		XRF			<	0.02092	%	Pd KA1F
Ag	0		XRF			<	0.02062	%	Ag KA1F
Li	0		INP						
In	0		XRF			<	0.03516	%	In LA1
Sc	0		XRF			<	0.01269	%	Sc KA1
Sb	0		XRF			<	0.09640	%	Sb LB1
Be	0		INP						
I	0		XRF			<	0.10047	%	I LB1
Cs	0		XRF			<	0.03707	%	Cs LA1
B	0		INP						
La	0		XRF			<	0.03640	%	La LA1
Ce	0		XRF			<	0.06901	%	Ce LB1
Pr	0		XRF			<	0.07451	%	Pr LB1

APPENDIX B. X-RAY FLUORESCENCE DATA FOR TANTALUM OXIDE CHIP

DEPARTMENT OF THE ARMY - BENET LABS - WATERVLIET ARSENAL 20-Oct-2001 15:53
SRS 3000 Siemens SemiQuant Interactive Evaluation Program
Sample Id. : TA2O5_STD_COTE Measured on 27-Sep-2001 11:16

-- Results --			-- XRF Concentrations --				
Ta	56.1 %	XRF	54.6	þ	0.26 %	Ta	LA1
O	23.4 %	XRF	22.8	þ	2.74 %	O	KA1
C	13.6 %	XRF	13.3	þ	8.63 %	C	KA1
Al	4.95 %	XRF	4.83	þ	0.122 %	Al	KA1
Na	0.442 %	XRF	0.431	þ	0.1697 %	Na	KA1
Si	0.305 %	XRF	0.297	þ	0.0569 %	Si	KA1
S	0.132 %	XRF	0.129	þ	0.0196 %	S	KA1
Fe	0.124 %	XRF	0.121	þ	0.0244 %	Fe	KA1
Er	0.109 %	XRF	0.106	þ	0.0541 %	Er	LB1
Cl	0.0989 %	XRF	0.0964	þ	0.02278 %	Cl	KA1
Tb	0.0835 %	XRF	0.0813	þ	0.05555 %	Tb	LA1
P	0.0721 %	XRF	0.0702	þ	0.02197 %	P	KA1
Ce	0.0672 %	XRF	0.0655	þ	0.06459 %	Ce	LB1
Sm	0.0662 %	XRF	0.0645	þ	0.03935 %	Sm	LA1
Ca	0.0634 %	XRF	0.0618	þ	0.02216 %	Ca	KA1
Mg	0.0573 %	XRF	0.0559	þ	0.05462 %	Mg	KA1
Ho	0.0566 %	XRF		<	0.12051 %	Ho	LB1
Yb	0.0513 %	XRF	0.0500	þ	0.04097 %	Yb	LA1
Mn	0.0508 %	XRF	0.0496	þ	0.01918 %	Mn	KA1
Th	0.0365 %	XRF	0.0356	þ	0.02490 %	Th	LB1
Pd	0.0332 %	XRF		<	0.06655 %	Pd	KA1F
Cr	0.0307 %	XRF	0.0299	þ	0.01676 %	Cr	KA1
Zn	0.0243 %	XRF	0.0237	þ	0.01377 %	Zn	KA1
Co	0.0223 %	XRF	0.0218	þ	0.01697 %	Co	KA1
Ti	0.0195 %	XRF	0.0190	þ	0.01363 %	Ti	KA1
V	0.0189 %	XRF	0.0184	þ	0.01387 %	V	KA1
Ni	0.0155 %	XRF		<	0.03222 %	Ni	KA1
Mo	0.0126 %	XRF	0.0123	þ	0.00856 %	Mo	KA1
Sc	0.0087 %	XRF		<	0.02106 %	Sc	KA1
K	0	XRF		<	0.02468 %	K	KA1
Ga	0	XRF		<	0.02368 %	Ga	KA1
Ge	0	XRF	0.1682	þ	0.02157 %	Ge	KA1
As	0	XRF		<	0.08701 %	As	KB1
Se	0	XRF ?	0.4331	þ	0.05586 %	Se	KA1
Br	0	XRF		<	0.03083 %	Br	KA1
Rb	0	XRF		<	0.04777 %	Rb	KA1
Sr	0	XRF		<	0.01005 %	Sr	KA1
Y	0	XRF		<	0.01441 %	Y	KA1
Zr	0	XRF		<	0.01020 %	Zr	KA1
Nb	0	XRF		<	0.00851 %	Nb	KA1
Ru	0	XRF		<	0.02759 %	Ru	KA1F
Rh	0	XRF		<	0.03976 %	Rh	KA1F
Li	0	INP					
Ag	0	XRF		<	0.02639 %	Ag	KA1F
Cd	0	XRF		<	0.03407 %	Cd	KA1F
In	0	XRF		<	0.03414 %	In	LA1
Sn	0	XRF		<	0.04099 %	Sn	LA1
Sb	0	XRF		<	0.08365 %	Sb	LB1
Te	0	XRF		<	0.04989 %	Te	LA1
I	0	XRF		<	0.09437 %	I	LB1
Cs	0	XRF		<	0.03705 %	Cs	LA1
Ba	0	XRF		<	0.03904 %	Ba	LA1
La	0	XRF		<	0.04410 %	La	LA1
Be	0	INP					

TECHNICAL REPORT INTERNAL DISTRIBUTION LIST

	NO. OF COPIES
TECHNICAL LIBRARY	
ATTN: AMSTA-AR-CCB-O	1
TECHNICAL PUBLICATIONS & EDITING SECTION	
ATTN: AMSTA-AR-CCB-O	3
PRODUCTION PLANNING & CONTROL DIVISION	
ATTN: SOSWV-ODP-Q, BLDG. 35	1

NOTE: PLEASE NOTIFY DIRECTOR, BENÉT LABORATORIES, ATTN: AMSTA-AR-CCB-O OF ADDRESS CHANGES.

TECHNICAL REPORT EXTERNAL DISTRIBUTION LIST

	NO. OF COPIES
DEFENSE TECHNICAL INFO CENTER ATTN: DTIC-OCA (ACQUISITIONS) 8725 JOHN J. KINGMAN ROAD STE 0944 FT. BELVOIR, VA 22060-6218	2
COMMANDER U.S. ARMY ARDEC ATTN: AMSTA-AR-WEE, BLDG. 3022 AMSTA-AR-AET-O, BLDG. 183 AMSTA-AR-FSA, BLDG. 61 AMSTA-AR-FSX AMSTA-AR-FSA-M, BLDG. 61 SO AMSTA-AR-WEL-TL, BLDG. 59 PICATINNY ARSENAL, NJ 07806-5000	 1 1 1 1 1 2
DIRECTOR U.S. ARMY RESEARCH LABORATORY ATTN: AMSRL-DD-T, BLDG. 305 ABERDEEN PROVING GROUND, MD 21005-5066	 1
DIRECTOR U.S. ARMY RESEARCH LABORATORY ATTN: AMSRL-WM-MB (DR. B. BURNS) ABERDEEN PROVING GROUND, MD 21005-5066	 1
CHIEF COMPOSITES & LIGHTWEIGHT STRUCTURES WEAPONS & MATLS RESEARCH DIRECT U.S. ARMY RESEARCH LABORATORY ATTN: AMSRL-WM-MB (DR. BRUCE FINK) ABERDEEN PROVING GROUND, MD 21005-5066	 1

	NO. OF COPIES
COMMANDER U.S. ARMY RESEARCH OFFICE ATTN: TECHNICAL LIBRARIAN P.O. BOX 12211 4300 S. MIAMI BOULEVARD RESEARCH TRIANGLE PARK, NC 27709-2211	 1
COMMANDER ROCK ISLAND ARSENAL ATTN: SIORI-SEM-L ROCK ISLAND, IL 61299-5001	 1
COMMANDER U.S. ARMY TANK-AUTMV R&D COMMAND ATTN: AMSTA-DDL (TECH LIBRARY) WARREN, MI 48397-5000	 1
COMMANDER U.S. MILITARY ACADEMY ATTN: DEPT OF CIVIL & MECH ENGR WEST POINT, NY 10966-1792	 1
U.S. ARMY AVIATION AND MISSILE COM REDSTONE SCIENTIFIC INFO CENTER ATTN: AMSAM-RD-OB-R (DOCUMENTS) REDSTONE ARSENAL, AL 35898-5000	 2
COMMANDER U.S. ARMY FOREIGN SCI & TECH CENTER ATTN: DRXST-SD 220 7TH STREET, N.E. CHARLOTTESVILLE, VA 22901	 1

NOTE: PLEASE NOTIFY COMMANDER, ARMAMENT RESEARCH, DEVELOPMENT, AND ENGINEERING CENTER, BENÉT LABORATORIES, CCAC, U.S. ARMY TANK-AUTOMOTIVE AND ARMAMENTS COMMAND, AMSTA-AR-CCB-O, WATERVLIET, NY 12189-4050 OF ADDRESS CHANGES.